University of Nevada, Reno

Influence of Ground Rotations on the Seismic Response of Building Structures

A thesis submitted in partial fulfillment of the requirements

for the degree of Master of Science in Civil and

Environmental Engineering

by

Rajan Aryal

Dr. David McCallen/Thesis Advisor

August, 2023

Abstract

Despite being studied for over four decades, seismic design codes still fail to incorporate ground rotations in analysis and design. The primary reason is the currently installed accelerometers' inability to measure ground rotation. In addition, installing sensors to measure ground rotations on a large scale is not feasible anytime soon. So, researchers have relied on indirect methods to derive rotational motions from translational records such as single station, multiple station procedures, and so on. However, these methods are unreliable during near-field events where the instruments can themselves rotate. This paper utilizes the application of high-performance computing (HPC) to extract ground rotations in light of these shortcomings. Due to recent advancements in HPC, the simulation of strong near-field events with high accuracy and high-frequency resolution is possible. This paper implements the newly developed Earthquake Simulation (EQSIM) fault-to-structure framework that uses an emerging GPU-based exascale computer platform. The simulation workflow consists of two steps. Initially, a 3D geophysical model representing a large domain of earth is developed, and the model is analyzed in SW4 fourth-order wave propagation code for two earthquake scenarios, Strike-slip and Reverse-thrust. Then, the ground motions extracted from the first step, including the rotational motion, are used to drive the engineering model of fixed-base and soil-structure interaction systems (SSI) through Domain Reduction Method (DRM). For this purpose, four canonical steel moment frame structures of 3-, 9-,20-, and 40-story are modeled in OpenSees. Finally, nonlinear time history analyses are performed to study the effect of ground rotation on the response of the considered structures. Results indicate that the ground rotations can significantly increase the buildings' inter-story drifts, producing

additional amplification when SSI is included. The impact of ground rotation is dictated by the fundamental natural frequency of the building along with the frequency and phase content of input motions.

Table of Contents

List of Tables

List of Figures

1.0 Introduction

It has been long recognized that ground motions generated by earthquakes can include ground rotations [1]. Despite this recognition, seismic analysis and design codes still fail to address ground rotations [2], primarily because of the lack of availability of a comprehensive database of recordings that can fully characterize rotations [1], [3]. Although modern technologies have allowed the measurement of ground rotation time histories on the research scale [3]–[6], it is still challenging to incorporate these technologies on a large scale. Therefore, the influence of ground rotations on the response of building structures has not been entirely assessed.

There is evidence of damage to structures caused by ground rotations in the work of a number of investigators [7]–[9]. Consequently, many researchers have studied the effect of ground rotation on structural response. For instance, using simplified shear building models, Gupta and Trifunac [10], [11] highlighted the significance of the contribution of the rotational motion to fixed-based buildings' response. Similarly, Kalkan and Graizer [10] presented the combined response spectrum for rotation and translation by studying the effect of rotational motions on a SDOF system with p-Δ effects. Likewise, Sheikhabadi [11] suggested that the contribution of ground rotation depends on structural height, irregularity, and seismic excitation. These studies have argued that ground rotations could adversely impact the response of structures. As a result, other studies explored the influence of near-fault rotational motions on the seismic demand of various structures. An example of this is a study by Trifunac [12], which focuses on the effect of near-fault strong ground rotations. Additionally, investigating the nonlinear response of a

two-story structure subjected to near-fault, fault-normal, and fault-parallel displacement, Jalali et al. [13] asserted that the combined action of horizontal, vertical, and rotational motions can amplify the building drifts. Moreover, Zembaty [14] found the impact of rotational components on the response of a 160 m tall RC chimney to be significant.

Recent studies have focused on examining the influence of rotational motions on multiple structures. An illustration would be the work by Bonkowski et al. [15], where they investigated the effect of strong ground rotations on 10- and 30-story structures using ETABS. Also, Basu et al. [16] analyzed various structures in SAP2000, subjected to translation, rotational, and torsional motions. Furthermore, Vicencio and Alexander [17] performed a parametric study using reduced-order mathematical building models on the influence of rotational motions and showed that they could significantly increase the displacement and acceleration response. Likewise, Vicencio and Alexander [18] found that soil-structure interaction (SSI) can produce additional amplification to the acceleration response obtained using rotational motions. At the same time, Fajardo and Papageorgiou [19] studied the effect of rotations induced by Rayleigh surface waves, including soil-structure interaction (SSI), unlike previous studies on rotational motions due to body waves. Very few studies [20], [21] have addressed the response of tall buildings due to rotational and torsional motions along with translational motions using a 3D geophysical model to simulate ground motions. By and large, all the previous studies have shown that rocking motions can increase the response of multi-story structures by up to 35 %. However, most of the earlier studies have utilized simplified models or linear analysis, and at most, the p-delta effect is included for multi-story buildings. Therefore, a comprehensive study that investigates the effect of near-field and far-field ground

rotations on small to tall structures, using detailed nonlinear finite element analysis is still missing. The focus of this paper is to fill in this gap.

Numerous methods to extract rotational motions to analyze their effects on structural responses are available in the literature. One example is the single station procedure (SSP), where the ground rotations are computed from three translational motions recorded at a single station. Here, the main principle is the decomposition of translational motions in body waves: P, SH, and SV. Many researchers [22]–[29] have used this concept to derive the rotational motions from translational motions recorded at a single station. However, SSP relies its assumptions on classical elasticity theories and has some limitations [16], [17], for example, (i) plane wave propagation, (ii) laterally homogeneous soil media, (iii) decomposition of horizontal motions into body and surface waves, and so on.

Another method of extracting rotational motions uses numerical finite difference approximation from the data of closely spaced stations, also called the dense array. This procedure, referred to as the multiple station procedure, is well documented in the literature [30]–[32]. Similarly, Spudich [33] presented the Geodetic Method (GM) similar to the multiple station procedure. In GM, the relative distance between the recording stations, distributed in a 3-D space, is expressed in terms of the displacement gradient matrix. However, the rotational motion obtained through GM leads to underestimating spectral ordinates at low periods [34].

On the other hand, Basu et al. [34] proposed the Acceleration Gradient Method (AGM), capable of extracting the free field rotational time series from dense array data. While

AGM can capture the high-frequency content lost in GM, it fails to do so after a threshold frequency [16]. Although the surface distribution method by Basu et al. [16] addresses the shortcomings of AGM, it has several conditions that are rarely satisfied, particularly for near-field earthquake records. In the strong near-field event, not only can the rotational motions derived from translational records miss the long period component of ground displacement, but the instruments are also subjected to rotation [21]. This can lead to unreliable rotational time histories.

Due to the limitations mentioned earlier, researchers are now inclined towards high-performance computing (HPC) to simulate earthquake scenarios and obtain ground motions in six degrees of freedom (three translational and three rotational). The concept of using simulations to extract translational motions and, more importantly, rotational motions has been used by many researchers. For example, Bouchon and Aki [35] simulated the time histories of ground strain and rotation, for strike-slip and dip-slip models, in the vicinity of earthquake faults. Many researchers have simulated synthetic rotational ground motion using a similar approach as Bouchon and Aki, using the discrete wavenumber method for simulation. For instance, Takeo[5] computed the time histories of ground rotational displacements of the largest earthquake during the 1997 swarm activity offshore of Ito Japan. Also, Mavroeidis and Papageorgiou [36] studied the characteristics of near-fault strains, rocking, and torsional components of ground motion. Additionally, using finite-fault simulation, Santoyo [39] estimated the time histories of near-fault ground strain and rotations of the 2011 Lorca earthquake, Spain (Mw 5.2). Similarly, Cao et al. [37] studied the effectiveness of physics-based simulation methods

to predict near-fault ground strains and rotations by comparing the simulated time histories with the observed one for the 2004 Mw 6.0 Parkfield, California earthquake.

With the confidence developed in simulated motions, different parametric studies have been conducted to establish a relationship between ground motions and source properties. For example, Cao et al. [38] performed a parametric analysis on the sensitivity of synthetically generated ground strains and rotations, using a kinematic source model of hypothetical strike-slip and dip-slip earthquakes, to variations in source properties such as fault type, magnitude, rupture velocity and so on. Based on the study by Cao et al. [38], Cao and Mavroeidis [39] have further investigated and compared the characteristics of synthetic motions, for instance, the time history of ground strain and rotation, with actual strike-slip earthquakes that are well documented: the 2004 Mw 6.0 Parkfield, 1979 Mw 6.5 Imperial Valley, and 1999 Mw 7.5 Izmit earthquakes. They performed the forward-ground motion simulation using a kinematic modeling approach.

Although previous studies have shown some discrepancies between simulated and actual motions, recent studies have shown reasonably good agreement [37]. Concurrently, the simulation of earthquake motions is moving toward the regional scale. This is due to the recent developments in HPC that have allowed the large-scale simulation of earthquake motions with high accuracy and at frequencies where the engineered structures are sensitive (5 to 10 Hz) [40]–[42]. Many researchers [20], [21], [43]–[45] have already utilized large-scale simulation to model seismic waveforms along with six components of ground motions. For example, Guidotti et al.[20] used a 3D geophysical model to simulate the near-fault time histories of ground rotations from the 2011 Mw 6.2

Christchurch, New Zealand earthquake dataset. Using synthetic motions, they addressed the response of tall structures to ground rotations. More recently, Wu et al. [21] simulated the ground motions for a hypothetical strike-slip earthquake using a newly developed Earthquake Simulation (EQSIM) framework [41], [42] and addressed the influence of rocking on various structures. Motivated by the work of Wu et al.[21], this paper explores the influence of rotational motions on moment frame structures for two hypothetical earthquakes including strike-slip and reverse-thrust faults.

EQSIM is a multidisciplinary fault-to-structure simulation workflow that couples an geophysics code with an engineering code to integrate earthquake hazards with seismic demand on structures. The simulation workflow is implemented in two steps. In the first step, a large-scale 3D geophysical model of the Earth is developed and analyzed in the SW4 fourth-order wave propagation code [46]. In the second step, the ground motions obtained from step 1 are used to drive the engineering model through code coupling. Two methods of code coupling are adopted. The first approach is weak coupling, where the fixed base models of buildings are developed. Another approach is strong coupling, where the SSI system is modeled using the Domain Reduction Method (DRM) approach by Bielek et al. [47]. Both models have been developed in OpenSees: a nonlinear finite element analysis platform [48].

This study investigates the contribution of rotational motions on building's overall response by defining two analysis setups for each coupling method: fixed base and DRM models. Initially, the fixed-base models are driven using surface translational motions only. As a result, the structures are excited purely horizontally and vertically, as seen in

Fig. 1a. Then the translational and rotational motions are simultaneously applied to the base of the structures. Unlike pure translational excitation, rotational motions induce the rocking of the structures, as shown in Fig. 1a. The rocking response combined with the translational response can amplify the overall response.

In contrast to the fixed base analysis, the complex three-dimensional wave fields with arbitrarily oriented body and surface waves are fed to the DRM model. The DRM analysis is crucial because the structures tend to show a rocking effect due to soil-structure interaction in addition to that of rotational motions, as seen in Fig. 1b. This combined effect can further amplify the response, thus producing a detrimental effect on structures. Also, the impact of rotation on fixed-base structures can be compared with that of the SSI system. For this purpose, nonlinear time history analyses are performed. Furthermore, the frequency content and phase difference of input motions are investigated.

2.0 Simulation workflow

The simulation workflow was implemented in two steps. First, a large-scale 3D geophysical model of a domain of earth was developed and analyzed in the SW4 fourth-order wave propagation code. The complex 3D motions were simulated, including the earthquake source and wave propagation path effects. Then, four canonical steel building models, 3-,9-,20-, and 40-story, were developed using two approaches in OpenSees. In the first approach, the traditional fixed-based models of the buildings were created. In the second approach, a model of reduced-size domain (called Domain Reduction Method model) equivalent to a small portion of the SW4 model was developed along with four

buildings. The DRM model explicitly allowed the consideration of soil-structure interaction.

Finally, nonlinear analyses were performed for both models with the input ground motions that were extracted from the SW4 geophysics model. While the input motions for the fixed-based models were vertical and horizontal motions computed at discrete points on the surface of the SW4 model, the input motions for the DRM model were complex three-dimensional wave fields consisting of arbitrarily oriented body waves and surface waves.

2.1 Earthquake scenarios

Two geophysical models with different rupture scenarios were analyzed in SW4 to simulate two different earthquakes: An M_w 7.0 generic fault strike-slip earthquake and an M_w 7.0 reverse-thrust fault earthquake. Both scenarios are similar in their modeling and were designed to produce realistic, broadband ground motions of high accuracy.

A large domain of size 100 km x 40 km x 30 km was modeled to capture a realistic rupture scenario. The kinematic rupture model by Graves and Pitarka [49] was used to generate the rupture because it allows the user to input the fault geometry and earthquake magnitude. This information was used to generate low-frequency and high-frequency ground motions. The minimum mesh size of the model was 8 m to ensure the frequency resolution of the obtained ground motions was up to 5 Hz. Subsequently, the earthquake event was initialized at 10 km in the FN direction and 27 km in the FP direction from the origin at a depth of 9 km. The fault rupture initiated at around 200 m below the surface. The event was initiated near the left side of the fault to observe the directivity effect (Fig.

2 a). Moreover, the material model included varying properties such as density, shear wave velocity, compressional wave velocity, and so on to represent soil inhomogeneity. The model contained a thin sedimentary basin of 600 m depth right next to the fault. The minimum shear wave velocity was equal to 320 m/s, and the variation of material properties were defined as follows.

$$V_p(d) = 1000 + 1.2d \ (m/s) \tag{1}$$

$$V_s(d) = 320 + \sqrt{19d} \ (m/s) \tag{2}$$

$$\rho(d) = 2140 + 0.125d \ (kg/m^3) \tag{3}$$

$$q_p(d) = 128 \tag{4}$$

$$q_s(d) = \ 64 \tag{5}$$

Where d is depth, V_p and V_s are compression and shear wave velocity, respectively, ρ is density, and q_p and q_s are quality factors for P-wave and S-wave, respectively.

The domain was divided into sub-domains of grid spacing 496 m, and the total number of sub-domains was 12060. The sub-domain starts at node 1, and the start location is given in Fig. 2b.
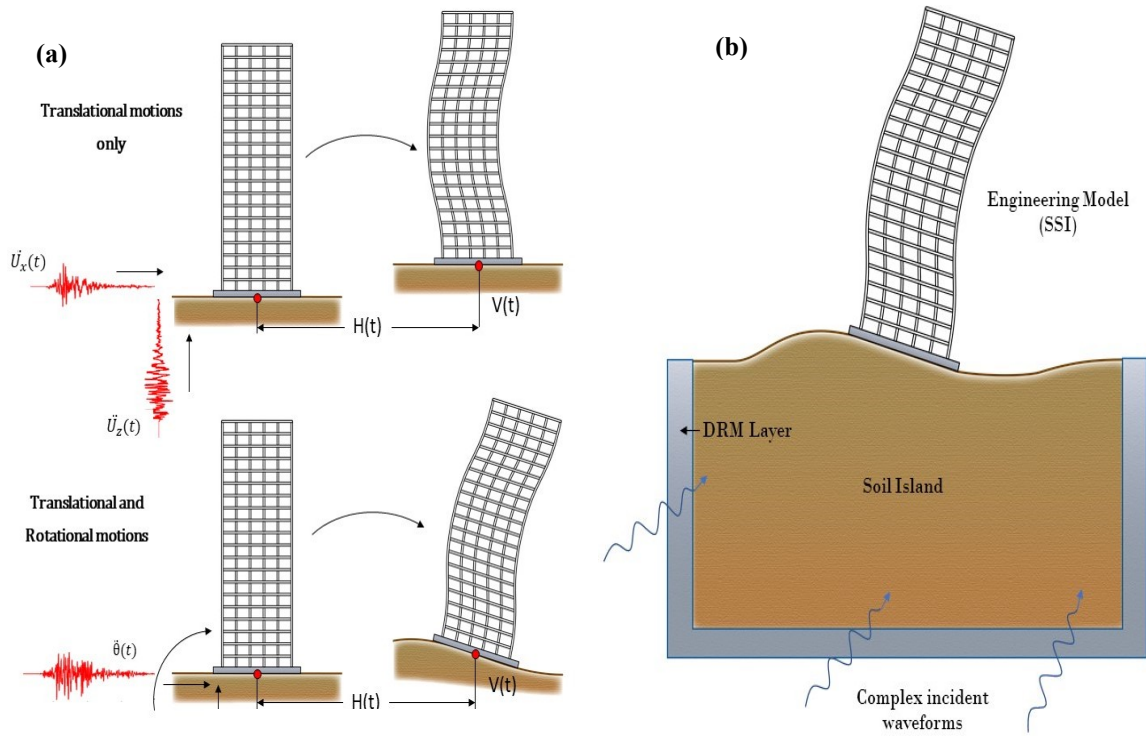
Fig. 1 A structure excited under translational and rotational motions (a) Fixed base and (b) DRM model with arbitrarily inclined waves
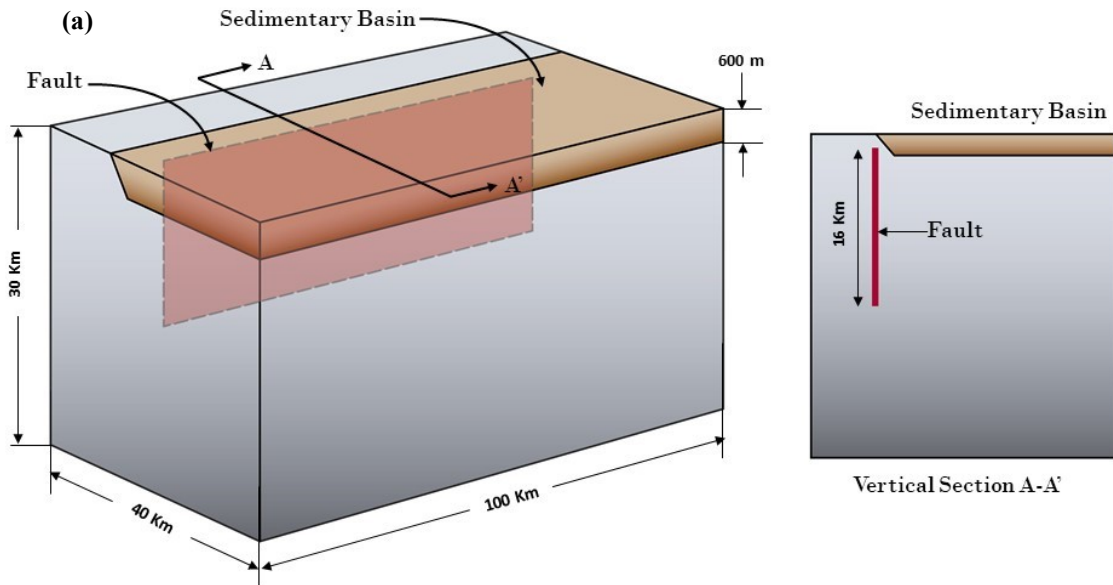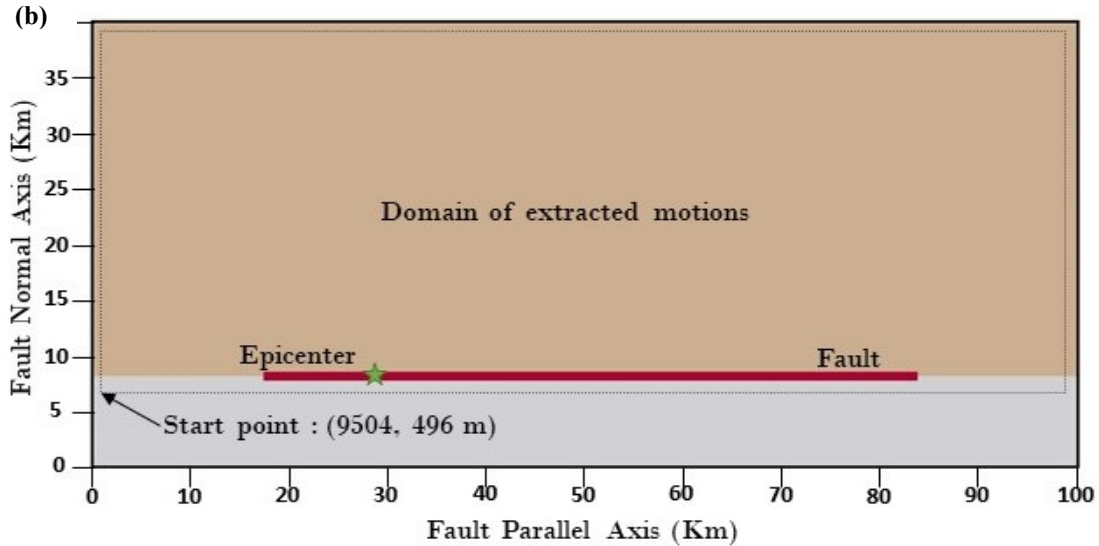
Fig. 2 3-D view (a) and Plan view (b) of the geophysics model for earthquake scenarios (EQ1 and EQ2)

2.1.1 Extraction of ground motions

Ground motions were calculated at a grid spacing of 496 m from the velocity output of

the SW4 simulation. Since the output of the SW4 model is velocity, appropriate

integration and differentiation were done to compute acceleration and displacement time

histories. The time step and the duration of extracted motions were 0.02257 and 50 sec,

respectively.

After extracting the translational motions, rotational motions were computed for each

sub-domain. For this purpose, a target surface is selected. Two points on the surface are

assigned with either x or y ordinate constant. These points are separated at a distance,

"L," which is also called the gauge length. Vertical velocities were then integrated to

obtain vertical displacement histories at the selected points, say U_{z1} and U_{z2} (see Fig. 3).

Subsequently; ground rotations were computed using equation 6. Note that the rotations

were insensitive to the chord length for the selected building footprint dimensions.

$$\theta_x(t) = (U_{z1} - U_{z2})/Chord\ Length \tag{6}$$

The obtained rotations were differentiated to calculate the velocity and acceleration time histories. Fig. 4 shows the rotational contour extracted from the SW4 simulation for both earthquake scenarios. Finally, complete sets of motions – translational motions in the x and y direction, vertical motions in the z direction, and rotational motions about the x and y direction— were obtained to proceed with the simulation. Complete ground motions for site 4985 of strike-slip are shown in Fig. 5.
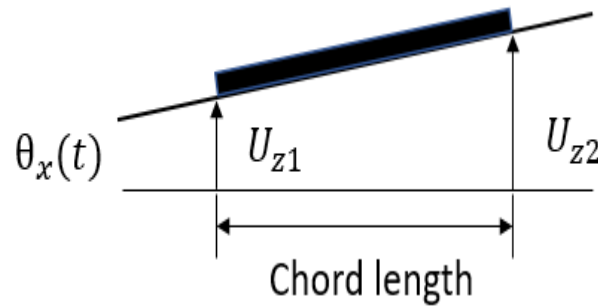
Fig. 3 Computation of rotational motions from vertical motions
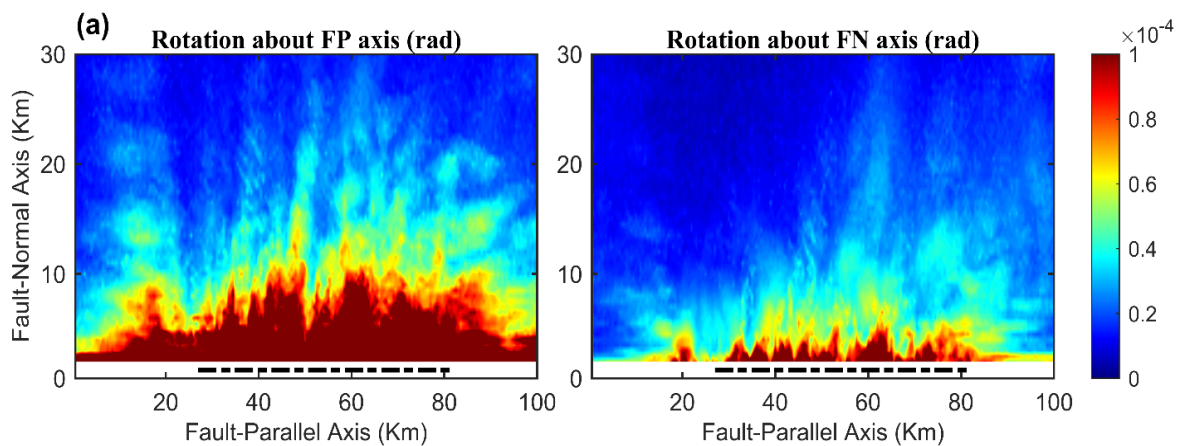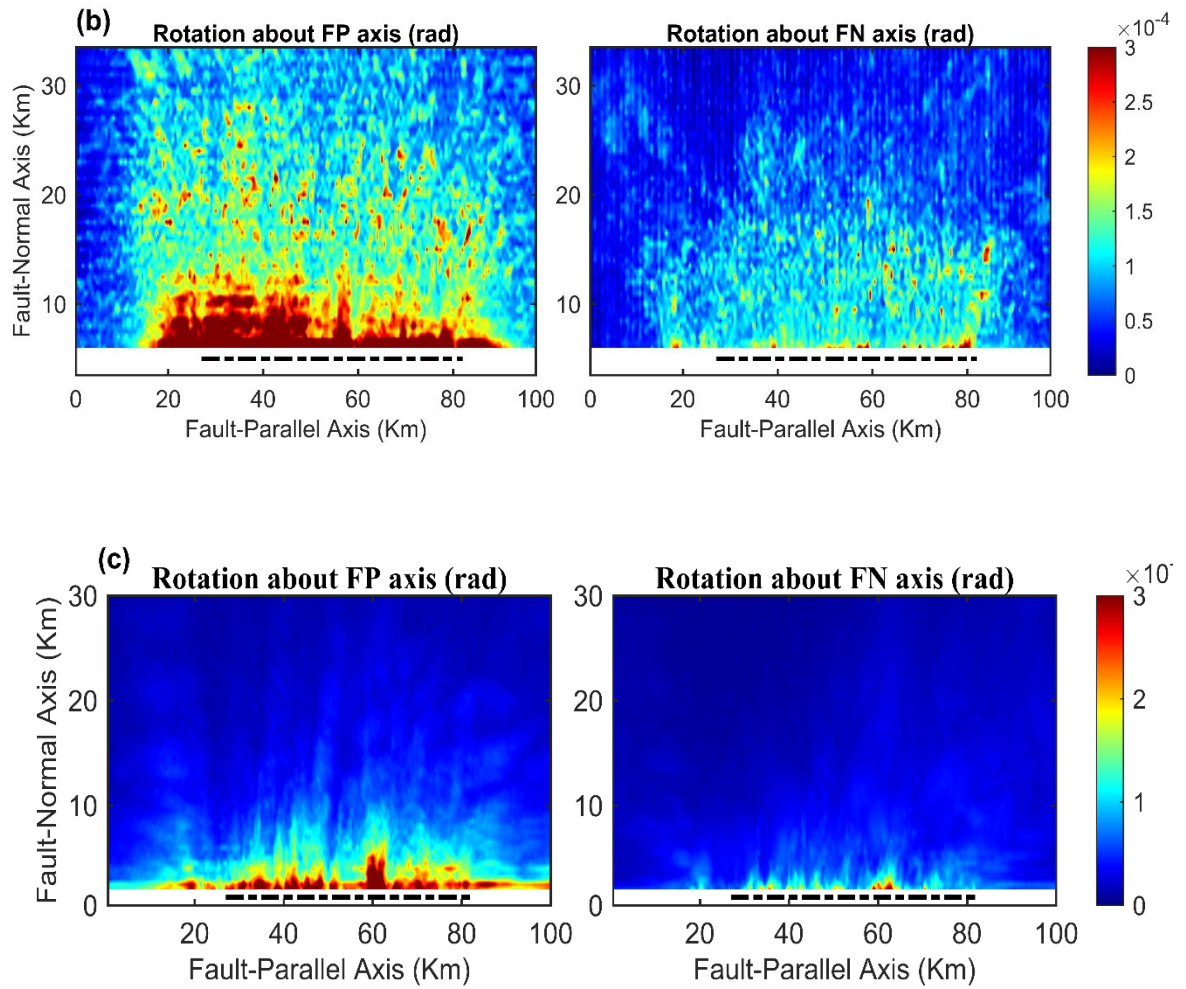
Fig. 4 Ground rotation contours about FP and FN axis for earthquake scenarios (a) Strike-slip, and (b) Thrust-fault (C) Strike-slip with same scale as Thrust-fault
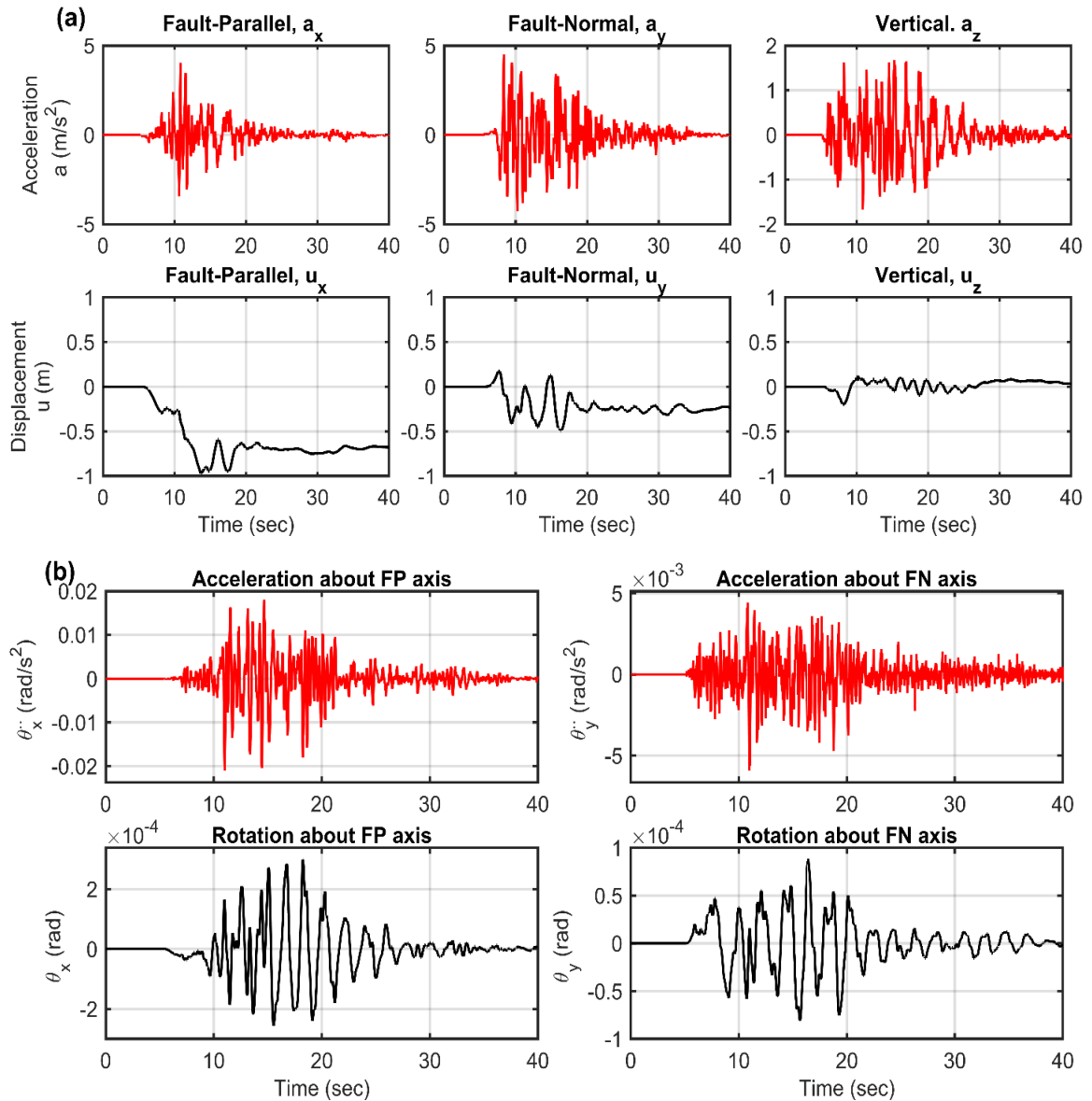
Fig. 5 Complete set of ground motions for subdomain no. 4985 (a) Translational motions (b) Rotational motions

2.1.2 Ground rotation verification

In this section, the ground rotation extracted in this study is verified comparing with the past studies. The magnitude of peak ground rotations observed is compared with past observations. Similarly, the relationship with elastic wave theory is used to verify the obtained ground rotations.

The peak ground rotations observed in previous studies are summarized in Table 1. As seen in Table 1, different methods have been developed to extract the ground rotation from translational motions. Recent studies are focused on direct measurement of rotations. The data provided in Table 1 has different origin and magnitude, However, the magnitude of ground rotation observed in this study falls in the same ballpark as the previously observed data.

An approximately linear relationship relating peak ground torsion (PGR$_z$) to peak translational ground velocity (PGV$_h$) and peak ground rocking (PGR$_h$) to peak vertical ground velocity (PGV$_z$) is suggested in the literature[20], [38], [50]–[52]. The relationship is given by equations 7 and 8.

Elastic wave theory states that seismic ground motion is assumed to be caused by harmonically propagating incident plane body and surface waves. This assumption has led to the formulation of the equations, for which c$_s$ corresponds to the phase velocity. However, recent studies have asserted that this assumption of plane wave propagation does not appropriately represents the near field region[38]. Therefore, c$_s$ is considered as a scaling factor that relates peak rotation to peak translation[20], [38].

$$\frac{PGV_h}{PGR_z} = 2c_s \qquad\qquad\qquad (7)$$

$$\frac{PGV_z}{PGR_h} = c_s \qquad\qquad\qquad (8)$$

where, c$_s$ is a scaling factor

Fig. 6 shows the scatter plot PGV_h versus PGR_z and Fig. 7 shows the scatter plot of PGV_z and PGR_h. As seen in these figures, the simulated data used in this study follows the linear relationship given in equations 8 and 9 for strike-slip and reverse-thrust earthquake. Moreover, it can be observed that the simulated data is in good agreement with the datasets observed in previous studies[20]. This provides confidence to move forward with the simulated ground motions.
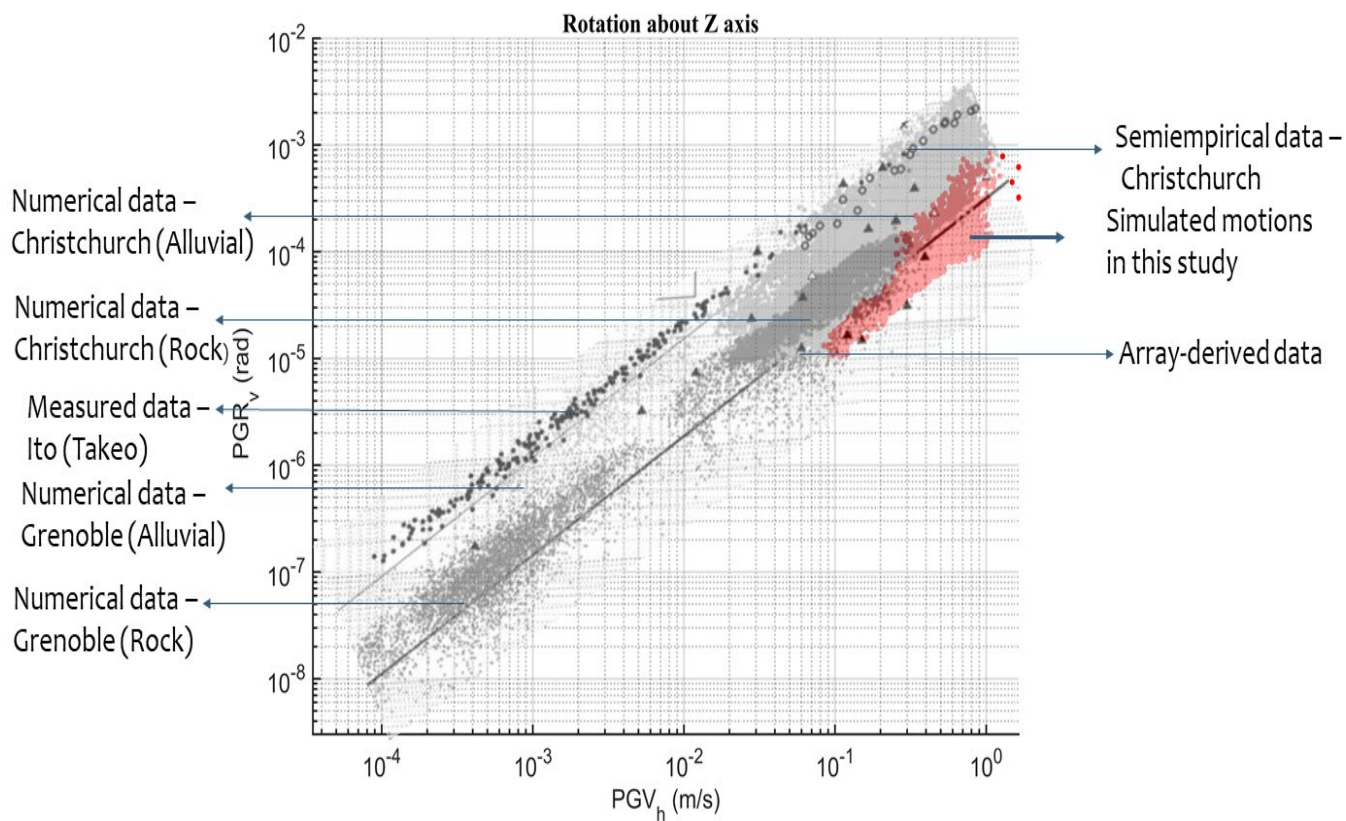
Fig. 6 PGR_z versus PGV_h in log scale of strike-slip earthquake and comparison with data set from Guidotti et al[20].

S.N.	Earthquake Type	Rotation (Rad)	Reference
1	30 Km long strike slip, Ms 6.9 El Centro earthquake	3.00E-04	Bouchon and Aki [35]
	Numerical Simultion with Fault at < 5 Km	7.00E-05	
2	El Centro differential array, Ms 6.9 strike-slip fault (within 5 km of fault)	1.00E-03	Niazi [30]
3	Earthquake recorded at strong-motion array in Taiwan, SMART -1, thrust type earthquake		Oliveria and Bolt [31]
	Ms 5.7, 30 km from fault	4.40E-06	
	Ms 6.7, 84 km from fault	5.70E-06	
	Ms 5.8, 22 km from fault	5.10E-06	
	Ms 5.6, 6 km from fault	5.70E-06	
	Ms 7.8, 79 km from fault	1.28E-05	
4	Rotational motions inferred from dense array observation of 1999 Chi-Chi Taiwan earthquake		Huang [32]
	Mw 7.6 Thrust-fault earthquake, 6 km from the fault	1.28E-05	
5	Rotational motions derived from Imperial valley differential array Mw 6.9 earthquake		Castellani and Boffi [26]
	Strike-slip earthquake, 18 Km from the fault	3.06E-05	
6	Rotational motions computed for Mw 6.0, 2004 Parkfield, California earthquake 8.8 km from the fault	6.89E-05	Spudich and Fletcher [50]
7	Rotational motions extracted from Eureka downhole array recordings during 2010 M6.5 Ferndale earthquake	6.00E-04	Graizer and Erol Kalkan [53]
8	3D Numerical study of a strike-slip event in Genoble valley Mw 6.0 event		Stupazzini and Igel [51]
	Viscoelastic soil material	1.89E-03	
	Nonlinear viscoelastic soil material	3.15E-03	
9	Finite fault analysis of Mw 5.2 Locra earthquake (Strike-slip fault)	2.00E-04	Santoyo [54]

Table 1 Literature data on magnitude of rotational component of ground rotation
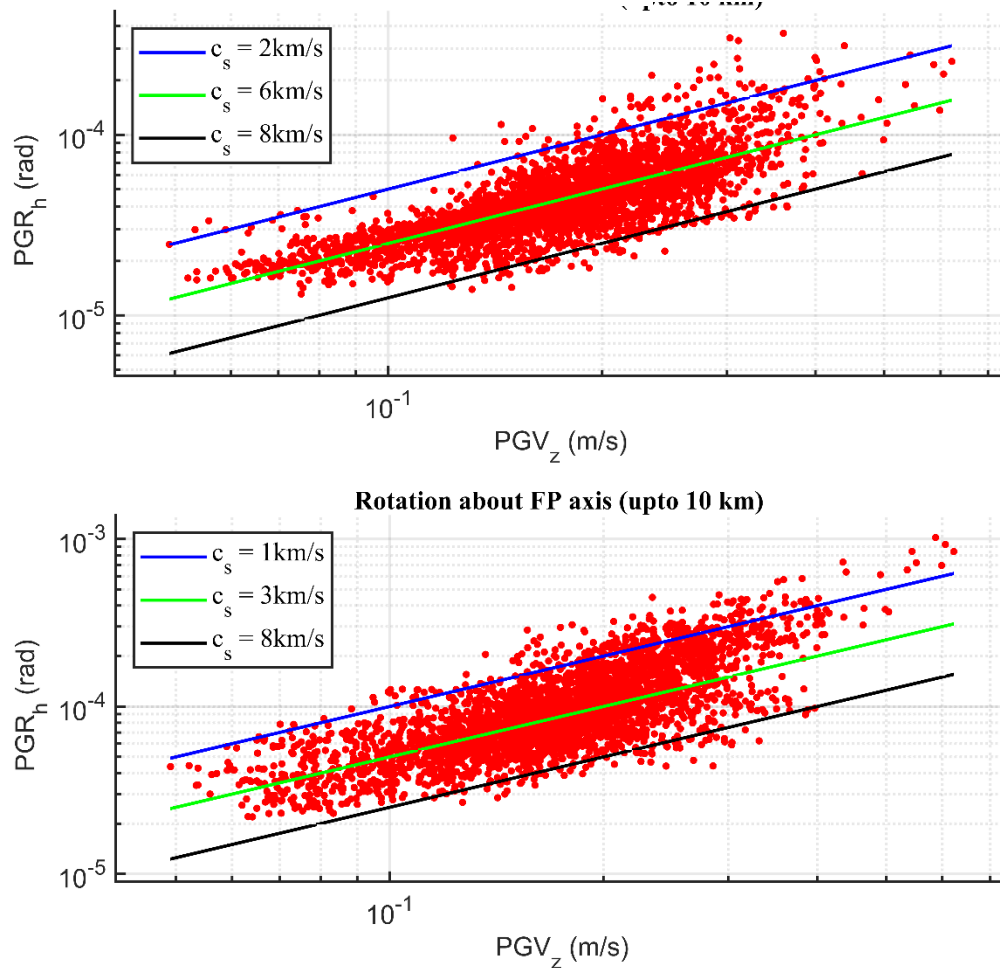
Fig. 7 PGR$_h$ versus PGV$_z$ in log scale for (a) strike-slip earthquake and (b) reverse-thrust earthquake

2.2 Building Models
2.2.1 Fixed Base Buildings

Four canonical moment resisting frame buildings of 3-, 9-, 20-, and 40 stories, shown in

Fig. 8, were considered. The period of the buildings ranged from 0.61 to 3.78 secs,

representing the buildings from low to tall heights. All the buildings were designed as per

ASCE 7-2016 and modeled in OpenSees. Then the building models were compared and

verified with other FEM codes, such as ESSI and SAP2000.The building models are fixed-base, two-dimensional models with three active degrees of freedom. Beams and columns are modeled using displacement-based beam elements with detailed fiber sections. Moreover, the nonlinearity was simulated using multiple techniques. The beams and columns are discretized into four elements to capture inelastic behavior. Also, the "Steel01" material with bilinear kinematic hardening is used to model the steel. Finally, the fiber section of every element is discretized into 32 fibers, with 11 fibers in the flange and 10 fibers in the web, thus simulating the yielding behavior of the steel. Other modeling and design details are described in Wu et al.[55] .

2.2.2 Domain Reduction Method

The DRM model was developed with three regions: a soil island in the interior region, a damping layer in the outer region, and a single-element layer between those two regions. The damping layer tentatively simulated the absorbing boundary to eliminate reflected waves into the soil island. Eventually, the canonical building models with spread

foundations were included in the DRM model to simulate the response of building models with soil-structure systems - in contrast to the fixed base response from the first analysis approach. The complex incident seismic waves from the SW4 model were fed to the DRM layer to obtain equivalent forces in OpenSees based on the equations in the literature [47]. Note that the building models were in 2D, but the DRM models were in 3D. As a result, 2D simplification of DRM was achieved by modeling a narrow model and verifying with a complete 3D model. The verification details can be found in Wu et al.[55]. Finally, the four buildings explained in sec 2.2.1 were included in the narrow

three-dimensional DRM model. To achieve this, mat foundations of different sizes were used.

The physical property of DRM models, including dimensions for soil island, size of mat foundation, and thickness of DRM layer, are provided in Table 2. In all DRM models, three layers of elements were used for the damping layer. Moreover, 8-node brick elements with elastic materials were used to simulate all components of the DRM model. The width of the soil island was different according to the story type to represent the bay width of each building. Additionally, the soil island's mesh sizes in translational and vertical directions were dictated by the foundation geometry and building sizes. However, only two elements were used in the out-of-plane direction of the model. Apart from the internal soil island, the DRM and damping layer mesh size was set constant at 8 m, similar to the mesh size of the SW4 geophysical model. Fig. 9 shows the geometry of a typical DRM model.

The material properties of the DRM models were set the same as that of the SW4 geophysical model using equivalent elastic properties based on the following equations.

$$G = \rho v_s^2 \tag{9}$$

$$E = 2(1 + \mu)G \tag{10}$$

$$\mu = (V_p^2 - 2V_s^2)/(2(V_p^2 - 2V_s^2)) \tag{11}$$

Rayleigh damping was used in DRM models in order to achieve a damping ratio equivalent to that of the SW4 model. For this, the equation in the literature [51], i.e., equation 12, was utilized. In order to achieve equivalent energy dissipation with the geophysics models, the equivalent damping ratio of the soil island and damping layer of

the DRM models was computed based on equations 1-5. The damping ratio was anchored

at periods of 1.0 sec and 0.1 sec so that a constant damping ratio was achieved for a

larger frequency range.

$$\xi = 1/(2q_s) \tag{12}$$

Table 2 The Geometry of the DRM models for all frames

Story Type	Geometry (L m x B m x H m)	Foundation size (L m x B m x T m)	DRM layer thickness (m)
3	170.68x 73.14 x 64	51.86 x 9.14 x 0.61	8
9	182.87 x 73.14 x 64	64.00 x 9.14 x 1.52	8
20	167.63 x 73.14 x 72	43.67 x 6.10 x 1.52	8
40	213.35 x 73.14 x 72	76.22 x 9.14 x 2.44	8

(a) 40-story   (b) 20-story   (c) 9-story   (d) 3-story
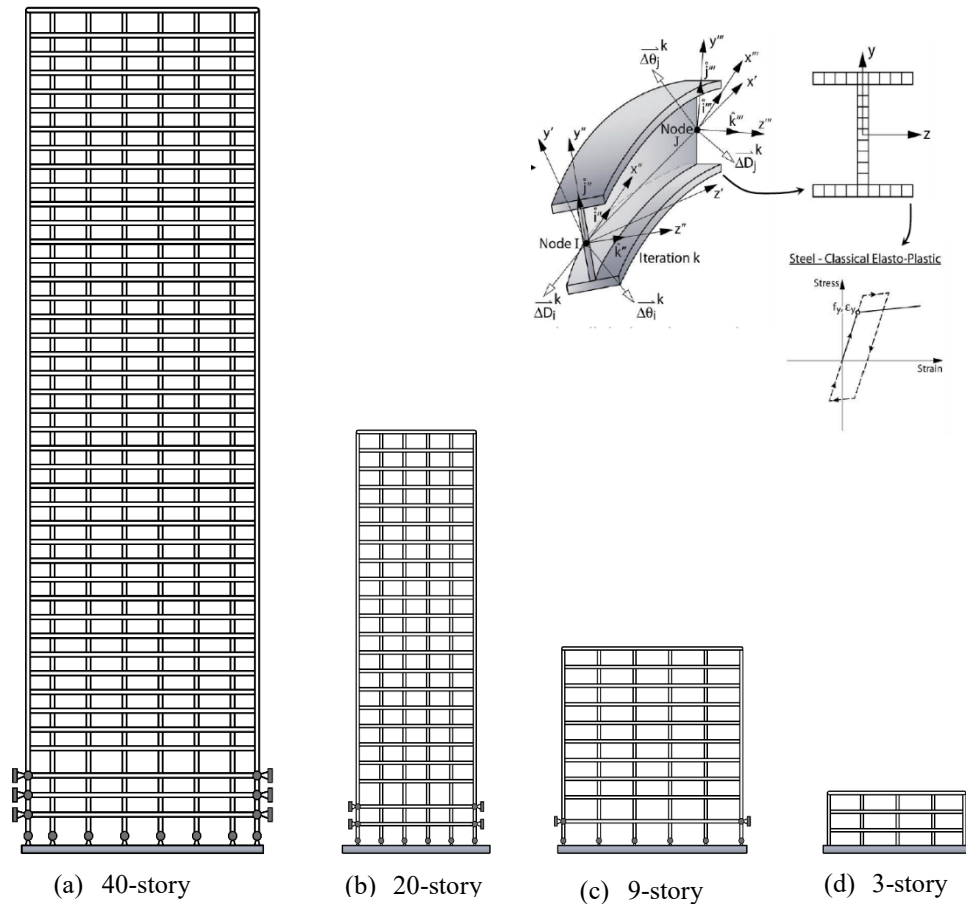
Fig. 8 Fixed-base models of four typical steel moment-frame buildings and plasticity model of steel
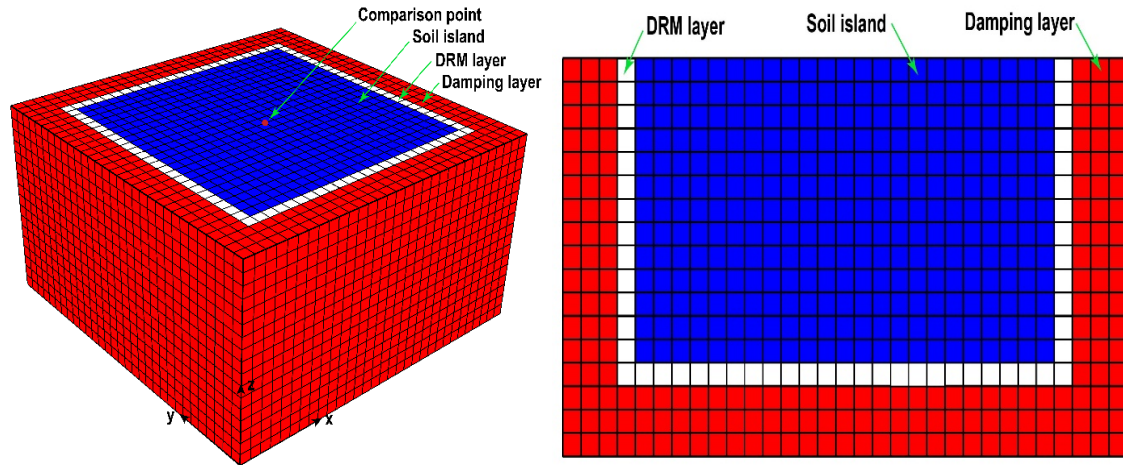
Fig. 9 DRM model in OpenSees (a) 3-D view and (b) elevation view

3.0 Influence of ground rotations on building's response

3.1 Analysis setup and performance parameter

This study investigates the effect of ground rotations on the response of moment frame buildings. So, the building models, both DRM and fixed-base models of four canonical steel frames, described in the preceding sections are subjected to simulated ground motions from the SW4 model. As mentioned earlier, due to the 2D simplification of both models, only in-plane (2D planar) excitations are used for performing the analysis. The in-plane excitation consists of translational (x), vertical (z), and rotational (θ) motions.

Since the mesh size of developed DRM models differ from that of the SW4 geophysical model, linear spline interpolation is used to extract the motions from SW4 model at the desired grid spacing. The DRM model with steel buildings are then analyzed under 2D planar motions. To drive the fixed-base models, the translational and vertical motions are computed at the center surface of the soil island.

Nonlinear time-history analyses are performed for 12,000 sites for both earthquake scenarios. For each sub-domain, the models are excited in the Fault-Normal (FN) and Fault-Parallel (FP) direction. During FN analysis, the input rotational acceleration is about the FN axis (see Fig. 2 b), and the input translational acceleration is along the FP axis. In contrast, during FP analysis, the rotational acceleration is about the FP axis, and the translational acceleration is along the FN axis. In both cases, the vertical acceleration is the same.

Finally, the analyses are performed, including the rotation (with R) and then excluding the rotation (No R) in FN and FP directions, respectively, to evaluate the effect of ground rotation. The time step (Δ t) of the analysis for strike-slip and reverse-thrust is 0.02256 sec and 0.002256 sec, respectively. Thus, the number of sub-steps was much more extensive for reverse-thrust than that for strike-slip. Note that the analyses are performed 1000 m away from the fault to the edge of the domain to avoid any singularity near or on the fault line.

The output of the analysis is the displacement time history for each floor of the building models. Peak inter-story drift (ID), which is the Peak relative distance divided by the height of the building, was then computed from the obtained displacement time history. The peak inter-story drift for cases including rotational excitation was denoted as ID_{WR}, and excluding rotational excitation was indicated as ID_{NR}. Percentage change in the inter-story drift, on every floor level, with and without rotation, was computed using equation 13.

$$\beta_i = (|ID|_{WR,i} - |ID|_{NR,i})/|ID|_{NR,i} \; x \; 100 \; \% \tag{13}$$

β_i = Change in drift for i^{th} level (%), $ID_{WR, i}$ = Inter-story drift including rotation for i^{th} floor level, and $ID_{WR, i}$ = Inter-story drift excluding rotation for i^{th} floor level

3.2 Effect on fixed base buildings

This section addresses changes in inter-story drifts due to ground rotations on fixed-base buildings for strike-slip and reverse-thrust earthquakes.

In a sub-domain(site), the β_i is the change in story drift for every floor level. The quantity of interest, the maximum change in drift amongst all the floor levels (hereafter referred to as β_{max}), is computed. β_{max} is calculated by taking the maximum value of the β_i—β_{max} ranges from negative to positive for the whole domain. Then, the subdomains are sorted based on the maximum to the minimum value of β_{max}. Results depicted in Fig. 10 and Fig. 11 are for the sub-domains with maximum change in the story drifts of each frame for the whole domain. Locations of these sub-domains are presented in Table 3 and Table 4.

For the strike-slip earthquake, Fig. 10a and Fig. 10b shows the inter-story drift along the height of the four fixed base steel frames in FN and FP directions, respectively. The red line indicates the inter-story drifts due to translational and rotational motions simultaneously. Similarly, the blue line represents the story drifts due to translational motions only.

In general, the inter-story drift of all structures increases when ground rotation is taken in account. FN analysis shows the maximum increase in drift is around 10 % for the 9-story frame. A similar increase of 9.54 % for 20-story and 9.12 % for 40-story frame are observed. However, the 3-story frame has a minor increase in the drift of about 3.6 % to that of other frames.

Furthermore, in FP analysis, the increase in the drift of 3-, 9- and 40-story frames are slightly higher than that of FN analysis; however, the increase in drift is significantly larger in the 20-story frame. The maximum value of β_{max} for the 20-story frame is approximately 21 % which is twice the increase compared to the FN analysis. Similar increase of 15% drift was observed by Guidotti et al.[20] for 28-story RC buildings. The drift magnification can be seen throughout the stories as seen in 20-story frame of FN analysis. Also, the magnification can produce new peak inter-story drift as seen in 20-story frame of FP analysis, which is more important as buildings are designed based on peak drift ratios.

Since the fundamental period of buildings varies, as given in Table 5, different responses are expected when the structures are subjected to ground motions. Not surprisingly, the sub-domains with the maximum rise in drifts differ for all the frames. Moreover, the magnitude of rotations associated with the maximum increase differs, i.e., 10^{-5} to 10^{-4} radians (see Table 3). Despite these dissimilarities, the increase in the drift of 9-, 20-, and 40-story buildings were in a similar range. These phenomena are similar to those reported by Bonkowski et al. [15], [56], and Vicencio et al. [17]. These findings suggest that peak ground rotation is not the only factor governing the response of structures.

Although the peak ground rotation is noticeably greater than that of FN analysis (see Table 3), the change in drift is in the same range except for the 20-story frame. This is primarily because the percentage increase is calculated relative to the response from translational motions. If the peak ground acceleration (PGA) of translational motions is small, then even a small ground rotation can cause a higher increase in response. In

contrast, if the PGA is extensive, then a large rotation may not cause a significant increase in the structural response. However, if the responses of structures subjected to rotational motions only are compared, then bigger rotation can be expected to increase the overall response. Section 4 of this paper provides some insights on this topic. By and large, the point of interest is the amplification of drift in comparison to translational motions.

For the reverse-thrust earthquake, Fig. 11a and Fig. 11b shows the inter-story drift trends of four steel frames in FN and FP directions, respectively. The results of the FN analysis are similar to those of the strike-slip earthquake. The drifts are magnified by 3 % in case of 3-story frames and rest of the frames have approximately 10 % increase in the drift.

On the contrary, the results of FP analysis show significant amplification in drift for 20- and 40- story frames. Table 4 shows that the peak ground rotation, which can induce the maximum increase in drifts, is sometimes greater and sometimes smaller than that of strike-slip in the case of FN analysis. In contrast, all the rotations are more significant in the case of FP analysis. Interestingly, the drift amplification of the 40-story frame is different compared to strike-slip despite having the peak rotation in the same range of 10^{-3} radians (see Table 4, FP analysis). The amplifications are more localized towards the lower stories as compared to strike-slip earthquake where drift amplifications are observed towards the upper stories. Similar observations of drift amplification at lower stories can be found in the works of Fajardo and Papageorgiou [19] for a 414 ft. tall steel frame structure.

Fig. 13a and Fig. 13b shows the contour depicting the variation in change in inter-story drift of whole domain of strike slip earthquake for rotation about FN and FP direction respectively. The red contour color shows the increase in drift and the blue contour color shows the decrease in drift. The figures indicate the rotation can increase as well as decrease the inter-story drifts of building structures. Moreover, the maximum increase is localized near fault in case of FN analysis. However, in case of FP analysis, there are sites away from fault line with increase in the drifts.

Fig. 14a and Fig. 14b shows the average of β_{max} for strike-slip and reverse-thrust earthquakes, respectively. The average increase in inter-story drift is low compared to the maximum increase, for all buildings, in case of both the earthquakes. In both cases, 20-story buildings appear to be more susceptible to ground rotation as they have the larger average increase in inter-story drift. This can result from the natural frequency of the 20-story frame being closer to the frequency content of the ground rotation.

By and large, these findings suggest that the ground motion characteristics, such as the frequency content of rotational motions, influence the response of the building. This paper investigates the frequency content of motions in section 4.

3.3 Effect on DRM Models

This section addresses changes in inter-story drifts due to ground rotation on DRM building models for a strike-slip earthquake. Section 3.2 suggests that the inter-story drift can be amplified for fixed based buildings. The maximum amplification can either occur at the location of peak-inter story drift or at any level other than peak drift. Since, the

design of structures are based on the peak inter-story drift (ID), the quantity of interest here is the maximum increase in peak drift(β_{peak}).

Fig. 12a and Fig. 12b show the amplification in inter-story drift due to the ground rotation on DRM models for strike-slip earthquakes for rotation about FN and FP axes respectively. For rotation about FN axis, the maximum amplification of 14.84 percent is observed in 40-story frame. The 3-, 9- and 20- story model has an increase in PID by 9.5%, 3.8%, and 7.8% respectively. Whereas for rotation about FP axis, 20-story model shows maximum amplification of 18.7%. The 3-, 9-, and 40-story model has an increase in ID of 5.4%, 15.5%, and 10.46% respectively. Note the domain location where maximum drift amplification is observed is not always the same for the DRM and fixed based model. This corroborates the influence of frequency content of rotation and its influence on the response of the buildings.

It is clearly evident that the DRM model can further magnify the peak ID in comparison to fixed-based model. The primary reason is that the effect of rocking is induced by the arbitrarily inclined waves. Moreover, soil-structure interaction (SSI) can add to the rocking effect. As a result, the peak ID is further magnified. For example, in case of rotation about the FP axis as seen in Fig. 12b, the rocking magnifies the inter-story drift leading to a new peak inter-story drift (ID). The DRM model can further amplify the newly obtained peak ID.

Similar to the fixed-base model, rocking can increase as well as decrease the inter-story drift ratio in DRM model. Even when the ground rotation does not induce any effect on the fixed-base building models, the DRM model can show some increase in ID. This can

be attributed to effect of soil-structure interaction.

Table 3 Maximum change of Inter-story drifts of all stories for FN and FP analysis, Strike-slip

Story Type	Axis of Rotation	Max change in drift (%)	Sub-domain	Rotation (rad)
3-story	FN	3.62	29	2.12E-05
	FP	3.98	3545	2.72E-04
9-story	FN	10.19	6904	1.58E-04
	FP	11.16	5404	4.09E-04
20-story	FN	9.54	6004	2.24E-04
	FP	20.81	5044	4.09E-04
40-story	FN	9.12	4684	1.86E-04
	FP	10.02	7084	1.02E-03

Table 5 Maximum change of Inter-story drifts of all stories for FN and FP analysis, Reverse-thrust

Story Type	Axis of Rotation	Max change in drift (%)	Sub-domain	Rotation (rad)
3-story	FN	3.01	351	3.58E-05
	FP	4.57	3231	2.95E-04
9-story	FN	9.40	8588	1.40E-04
	FP	9.64	9191	6.06E-04
20-story	FN	9.69	9325	4.66E-04
	FP	16.13	5841	6.00E-04
40-story	FN	10.46	9861	1.76E-04
	FP	28.47	9526	1.18E-03

Table 4. First three fundamental modes of vibration of 3-, 9-, 20-, and 40-story frame

Mode	Story Type			
	3-story	9-story	20-story	40-story
1st mode (sec)	0.606	2.138	2.681	3.787
2nd mode (sec)	0.191	0.734	0.927	1.365
3rd mode (sec)	0.097	0.41	0.536	0.814

Fig. 10 Inter-story drift trends for 3-,9-,20-and 40-story buildings with and without rotation for subdomains with maximum change in ID (a) Rotation about FN axis and (b) Rotation about FP axis (Strike-slip)

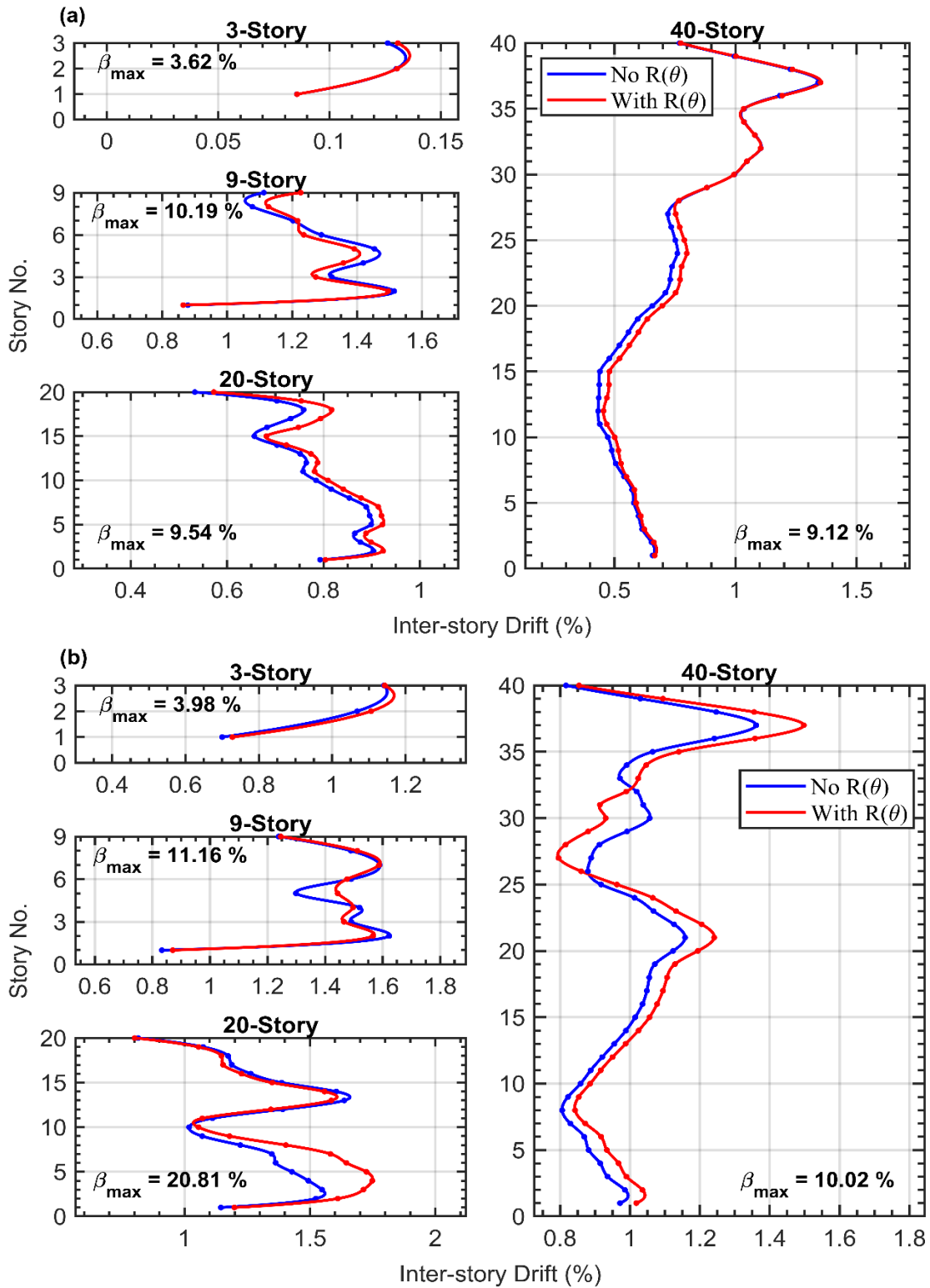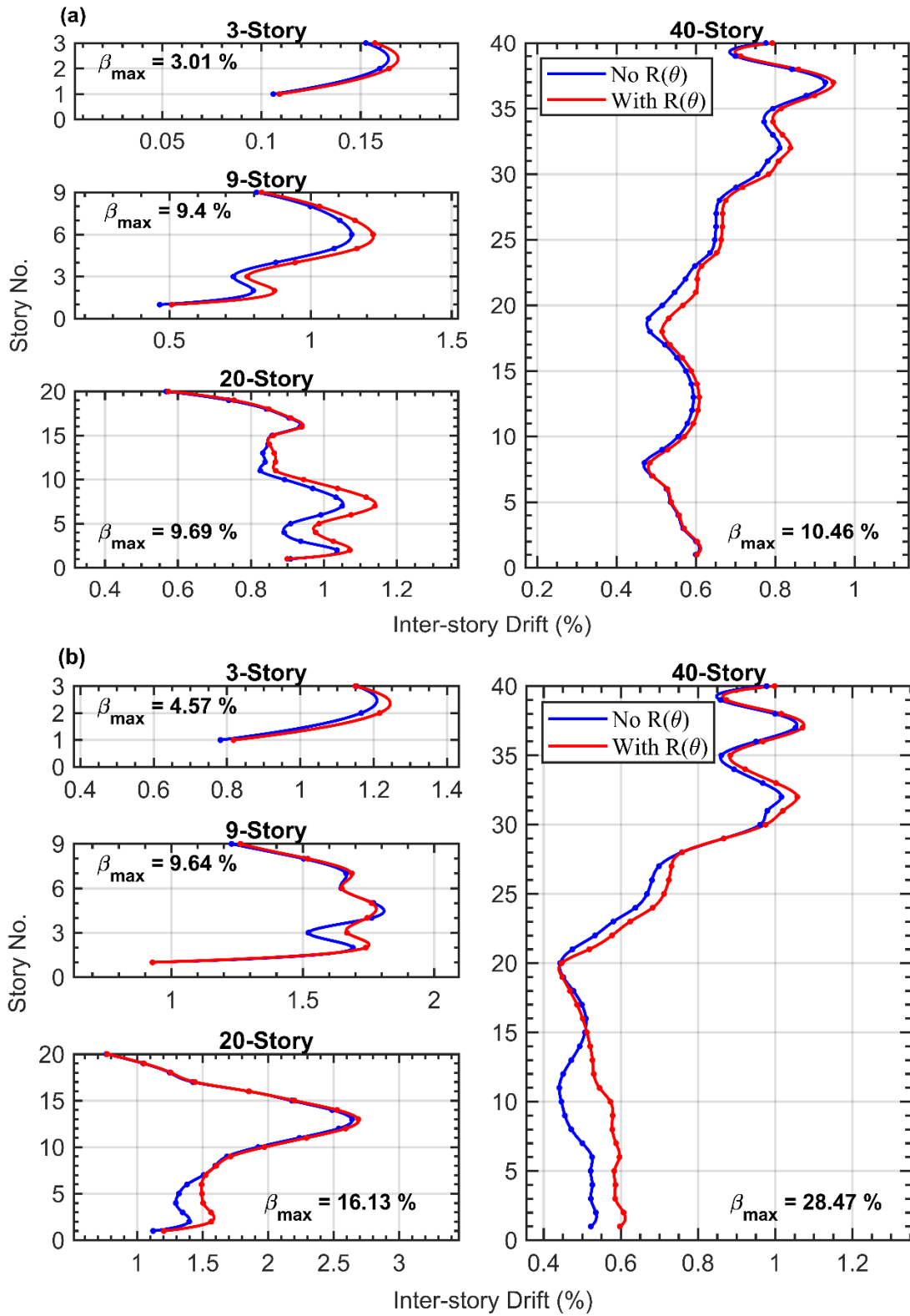*Fig. 11 Inter-story drift trends for 3-,9-,20-and 40-story buildings with and without rotation for subdomains with maximum change in ID (a) Rotation about FN axis and (b) Rotation about FP*

Fig. 12 Inter-story drift trends for 3-,9-,20-and 40-story buildings with and without rotation for fixed-base and DRM models(a) Rotation about FN axis and (b) Rotation about FP axis (Strike-slip)
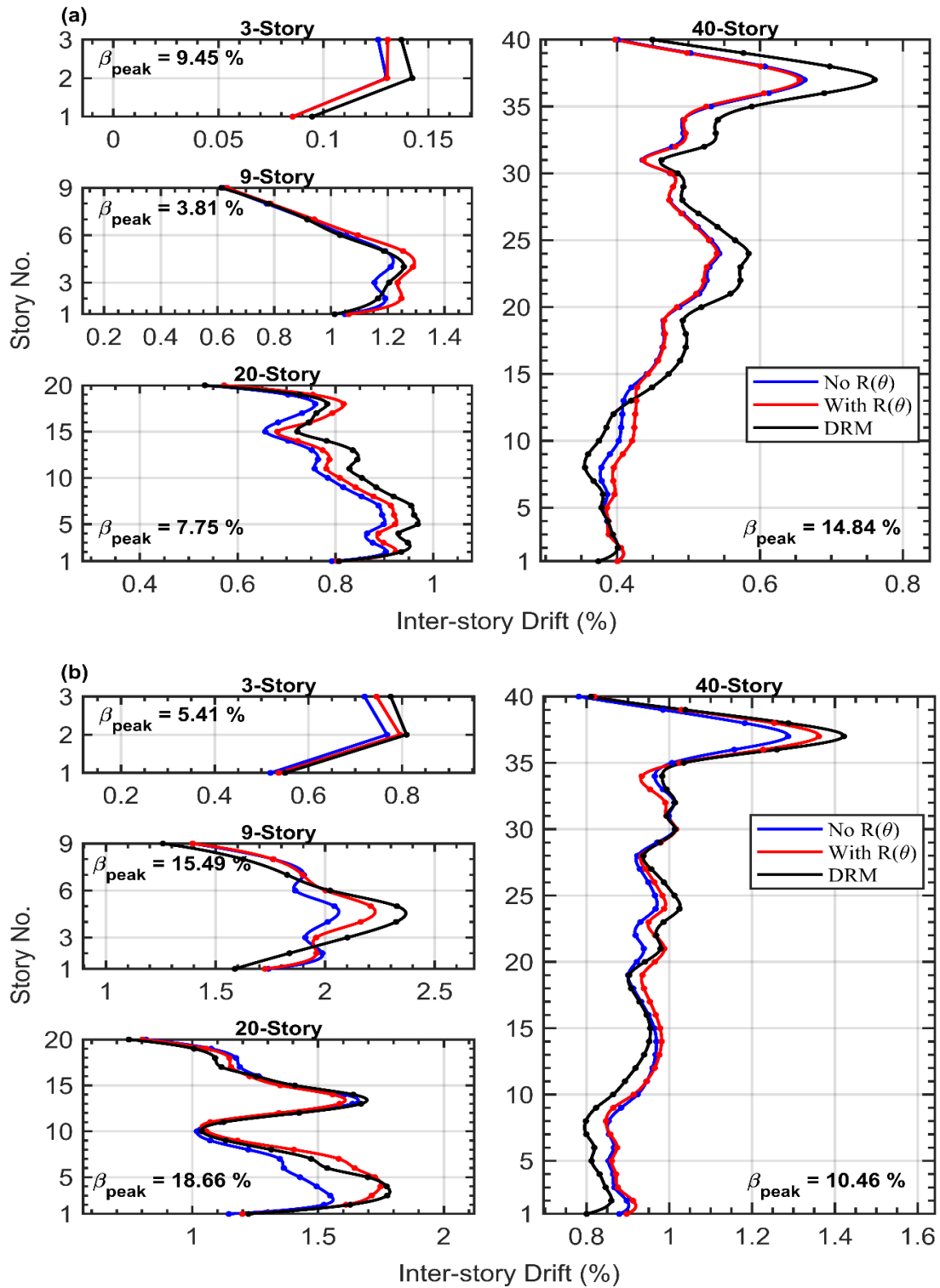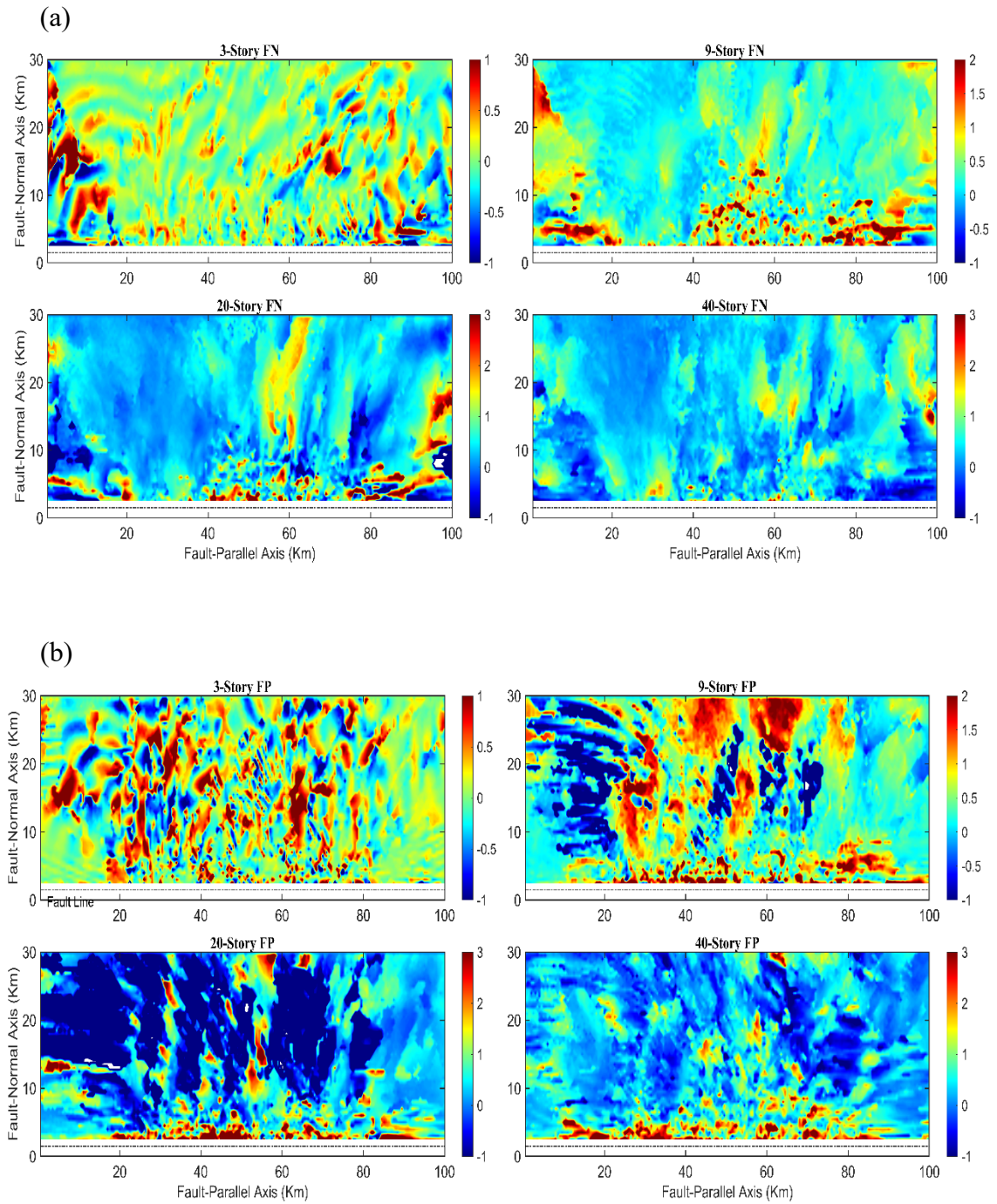
(a)

(b)

Fig. 13 Contour depicting the variation in ID for whole domain of Strike-slip earthquake (a) Rotation about FN axis (b) Rotation about FP axis
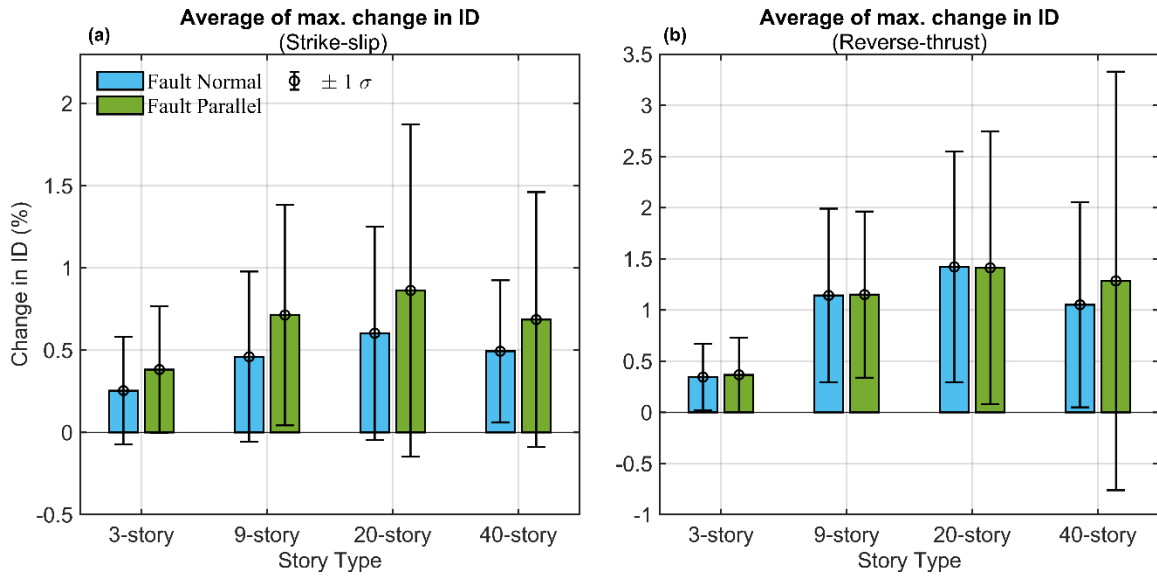
Fig. 14 Average and standard deviation of maximum change in ID for (a) Strike-slip earthquake, and (b) Reverse-thrust earthquake

Table 6 Effect of rotation on overall response of different structures from the literature

SN	Structure Type	Response Parameter	Contribution of rotation	References
1	28-story RCC building	Drift	15%	[20]
2	4-story base isolated building	Displacement	15%	[16]
3	4-story fixed base building	Displacement	2%	[16]
4	5-story building	Story Shear	43%	[11]
5	10-story building	Story Shear	21%	[11]
6	10-story building	Story Shear	16%	[15]
		Overturning Moment	7%	[15]
7	30-story building	Story Shear	5%	[15]
		Overturning Moment	15%	[15]
8	160m high R/C Chimney	Bending moment at base	65%	[56]
9	Two story building with SSI	Displacement	35%	[17]

4.0 Ground motion characteristics and response of structures

In this section, the characteristics of the input motions are evaluated in relation to the response of structures. As noted in the previous section, the rotation motion can increase as well as decrease the response of the structure. Similar observations are made in the literature [15]. This behavior can be associated with the frequency content, phase difference [57], and the magnitude of the input rotational motions.

Fig. 15 shows the response spectra of rotational motions about the FP and FN axis. Many variations in the amplitude and frequency content of response can be observed. Note that the response spectra are displayed for motions within 3 km of the fault because the effect of rotation is maximum in this region for all considered structures.

4.1 Frequency content of input motions

The mean period (T_m) is selected to study the frequency content of input motions. Many researchers have adopted T_m as a measure of the frequency content of strong motion [58]–[61]. T_m is calculated using the following expression by Rathje [62]:

$$T_m = \frac{\Sigma_i \, c_i^2 \, x \frac{1}{f_i}}{\Sigma_i \, c_i^2} \qquad \text{for 0.25 Hz} \leq f_i \leq \text{20 Hz, } \Delta f \quad \leq \text{0.05 Hz} \qquad (14)$$

Where f_i = discrete fast Fourier transform (FFT) frequencies in the range 0.25 to 20 Hz, C_i = Fourier amplitudes coefficients; Δf = frequency interval used in FFT.

After performing the fast Fourier transform of all ground motions, the amplitude spectrum is obtained. Fig. 16 depicts the acceleration time history of translational and rotational motion along with the respective Fourier amplitude spectrum and response spectrum of sub-domain 5044. Similarly, Fig. 17 shows all the information mentioned

earlier for sub-domain 5404. Then, the range of the mean period and its average value is computed. Table 5 shows the lower, upper, and average mean period of the considered translational and rotational motions about the FN and FP axes. Also, the first three fundamental periods of all the structures are shown in Table 5.

The structures are subjected to rotational motion alone to investigate the relation between the frequency content of rotation and its response. Fig. 18 shows that, in the case of a 3-story frame, the maximum roof displacement tends to increase as the Tm approaches the first mode of the structure. Moreover, the contribution of higher modes appears to be small. This phenomenon is happening because the mean period of input rotation is close to the first mode of the building, and there are very few motions with a mean period close to the second mode. Nevertheless, the contribution of the second mode is not as pronounced as the first mode.

On the contrary, in the case of a 9-story, the first mode is larger than the upper range of the mean period of the rotational motions (see Table 7). Therefore, the contribution of the higher mode can be observed in Fig. 18. When the mean period is close to the second and third modes, the maximum response is observed. Most of the high responses are in between the second and third modes.

Table 7 Upper range, lower range, and average of Mean period of input translational and rotational motions (Strike-slip earthquake)

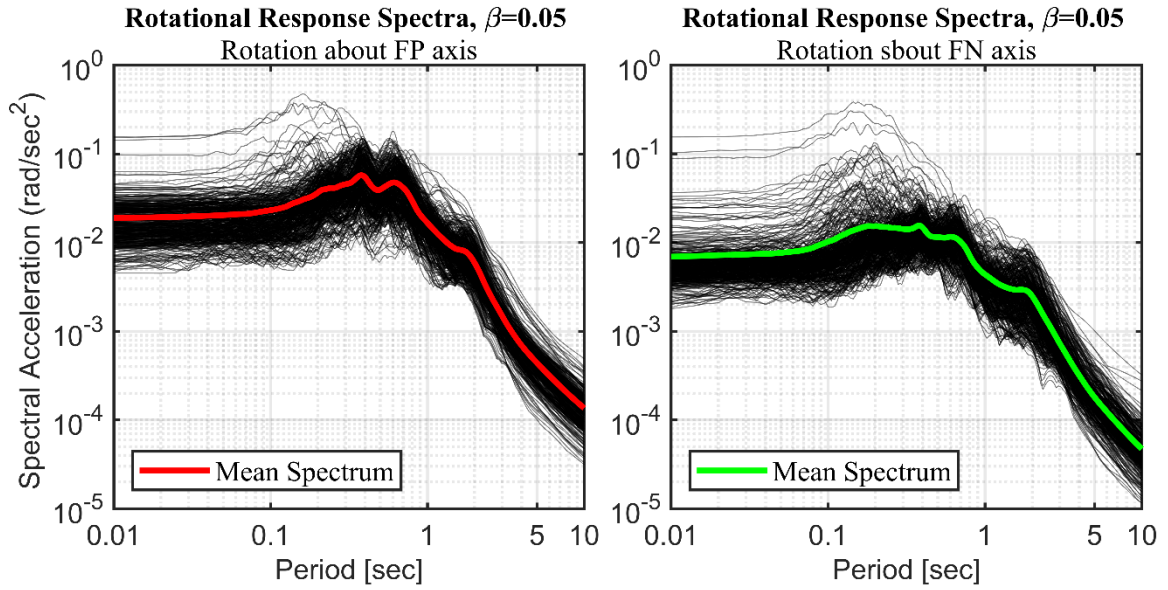| Mean Period	Rotation		Translation	
	About FN axis	About FP axis	About FN axis	About FP axis
Min. T_m (sec)	0.1594	0.1955	0.4858	0.3006
Max. T_m (sec)	0.848	0.8924	1.4907	1.6278
Avg. T_m (sec)	0.3291	0.4168	0.9166	0.8575

Fig. 15 Rotational response spectra for motions within 3 km of the fault for Strike-slip earthquake

Fig. 16 Acceleration time history, Fourier amplitude spectrum and Response spectrum for Translational and Rotational motions of Sub-domain 5044 (Strike-slip)
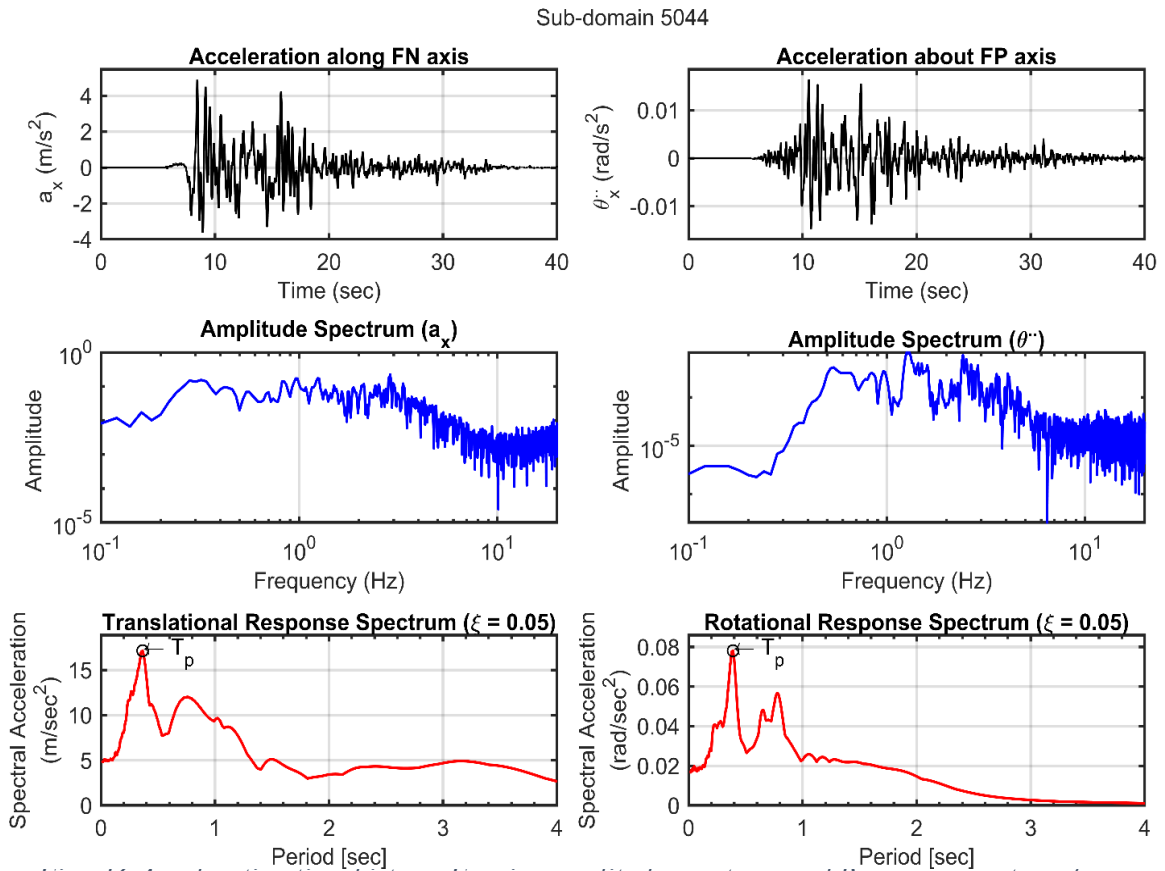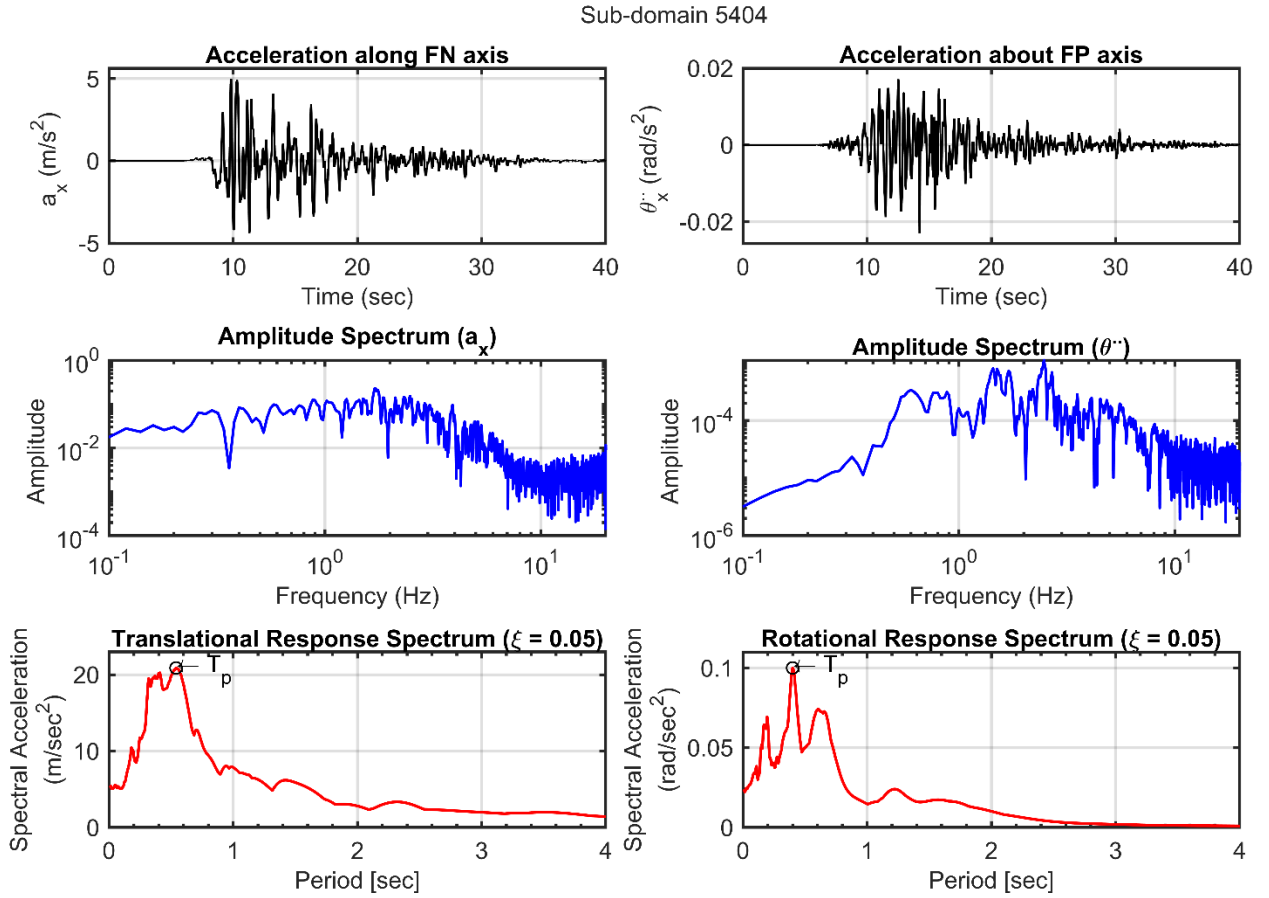
Fig. 17 Acceleration time history, Fourier amplitude spectrum and Response spectrum for Translational and Rotational motions of Sub-domain 5404 (Strike-slip)
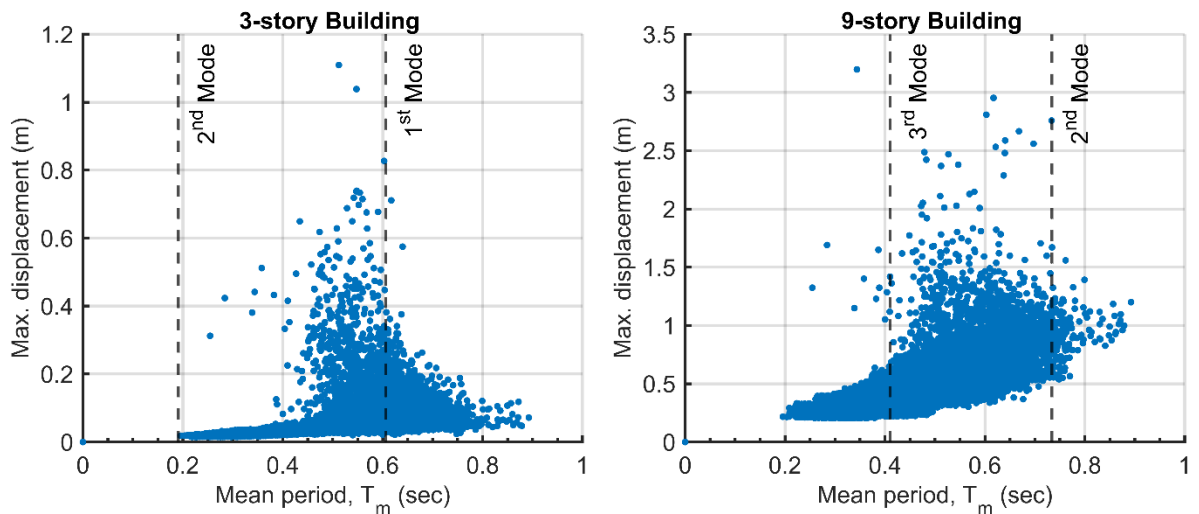

Fig. 18 Maximum roof displacement vs Mean period of input rotational motions for 3-story and 9-story buildings subjected to rotational motions only. (Strike-slip)

4.2 Phase difference of input motions

This section explains the role of differences in phase content of input rotation and translational motions on the response of the structures. For this purpose, the equation of motion subjected to roto-translational motion and the response of the 20-story building are selected.

Let us consider an SDOF system subjected to translational and rotational motions. The equation of motion is given by the following equation.

$$m\ddot{u}(t) + c\dot{u}(t) + ku(t) = -m\ddot{u}_g(t) - mh\ddot{\theta}(t) \qquad (13)$$

Where m, c, and k are the system's mass, damping coefficient, and stiffness. Similarly, $\ddot{u}(t)$, $\dot{u}(t)$, and $u(t)$ are acceleration, velocity, and displacement responses of the SDOF system. $\ddot{u}_g(t)$ and $\ddot{\theta}(t)$ are translational and rotational ground acceleration.

Let's say the SDOF system is excited by a combination of translational and rotational motions. The total response of the system is a combination of responses due to translational excitation and rotational excitation. Since they have different frequency content, as suggested by the previous section, the response due to translational motion alone is different from that of rotation (see Fig. 17 and Fig. 18). Moreover, the individual response can be in phase with each other, thus increasing the effect of rotation. Alternatively, they can be out of phase, therefore decreasing the effect of rotation.

This phenomenon is illustrated by considering the rotational motions of two subdomains, that is # 5044 and # 5404. These domains have the same peak ground rotation but different frequency parameters. As a result, the dominance of PGR is ruled out. Then, the

response of the 20-story building is considered for this illustration. As seen in Fig. 19, the total displacement response tends to be amplified when the rotational response is in phase with translation. In contrast, as depicted in Fig. 20, the total displacement appears to be unchanged due to out-of-phase rotation.
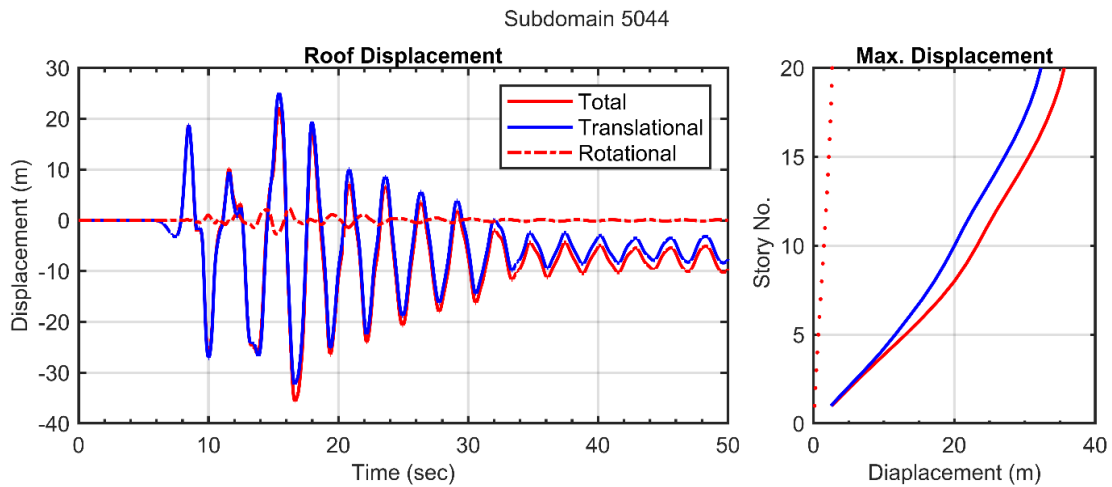

Fig. 20 Displacement response of 20-story building subjected to rotation, translation and roto-translational motions for subdomain 5044.
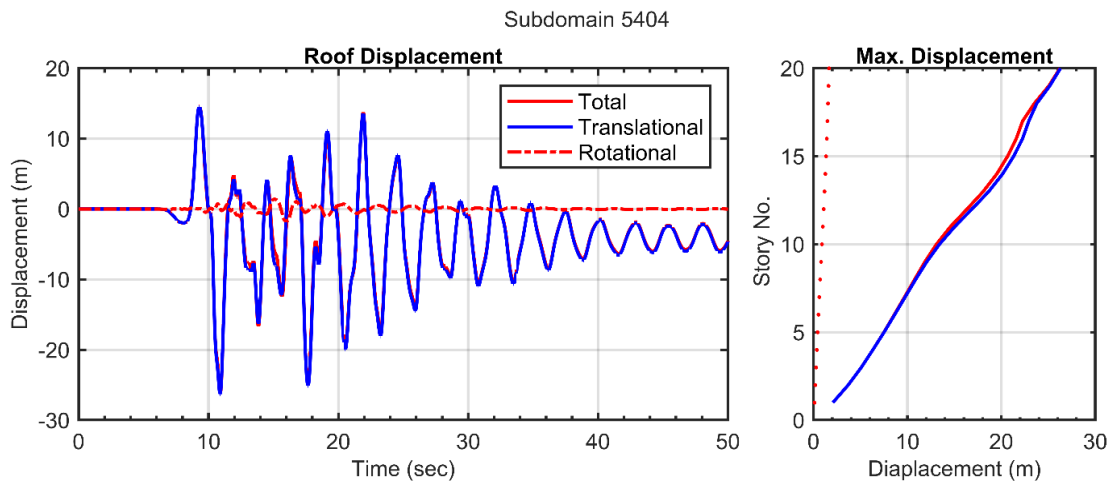

Fig. 19 Displacement response of 20-story building subjected to rotation, translation and roto-translational motions for subdomain 5404.

5.0 Conclusion

This paper investigates the influence of the rotational component of ground motions on the response of moment frame structures. The rotational motions are extracted using high-performance simulation. For this purpose, a recently developed computational workflow, i.e., EQSIM, is implemented in two steps. Firstly, a large-scale 3D geophysical model, which considers earthquake source and wave propagation, of a domain of Earth is simulated in the SW4 fourth-order finite difference code. Two earthquake scenarios, including Strike-slip and Reverse-thrust earthquakes, are simulated in the first step. Then, the regional geophysical model is coupled with the local engineering models using two approaches. In the first approach, fixed-base models of 3-,9-,20-, and 40-story moment frame buildings are modeled in the OpenSees. Similarly, in the second approach, the previously defined buildings are modeled, including the soil-structure interaction system using Domain Reduction Method (DRM).

Extensive nonlinear time history analyses were performed using the motions obtained from the geophysical models on the four-moment frame structures. The results indicate that the rotational motions can significantly amplify the inter-story drifts (ID) of the structure. For example, the increase in the ID of the 20-story building is about 21 % for a Strike-slip earthquake. Also, the increase in the ID of the 40-story building is about 28 % for a Dip-slip earthquake. The percentage increase in response is closely dependent on the magnitude of translational motions and its response.

Soil-structure interaction and inclined body waves, incorporated via the Domain Reduction method, can further amplify the inter-story drifts trends even for the small

buildings. DRM model amplifies the peak inter-story drift to a new level. Even in small frames such as 3-and 9-story frame a 10-15.5% increase in peak drift is observed. The maximum increase of approx. 19% is observed in a 20-story frame. Also, in cases where a fixed based model does not produce any amplification, application of DRM can result in observable rotation impact on drift. This is primarily due to the effect of soil structure interaction. The results of the DRM model indicate that rotations can be more damaging to the structures as peak-inter story drifts are further magnified as compared to fixed base models.

The results also suggest that the frequency content of the rotational motions largely influences the response of the structure. When the mean period of rotational motions is close to the fundamental period of the building, the response tends to increase. For instance, the displacement of a 3-story building seems to increase for input motions with a mean period close to the first mode. Similarly, the displacement of 9-story buildings tends to increase for motions with a mean period close to the second and third modes. Similar observations are made for 20- and 40-story frames.

Moreover, the findings show the significance of the phase content of input motions. The response tends to amplify if rotational motion is in phase with the translational motions, However, if they are out of phase the effect of ground rotation is minimal, and in some cases the overall response of the structures is decreased.

The extensive analysis conducted in this study highlights the significance of the contribution of rotational motions on the overall response of structures. Since ground rotation can significantly increase the inter-story drift demand, modern design safety

standards should address the rotational motions. Especially in case of performance-based design, where the performance of structures are critical, a 21% increase in drift can lead the structure from severe damage to collapse state.

7.0 References

[1] W. H. K. Lee, M. Celebi, M. I. Todorovska, and H. Igel, "Introduction to the special issue on rotational seismology and engineering applications," *Bull. Seismol. Soc. Am.*, vol. 99, no. 2B, pp. 945–957, 2009.

[2] M. D. Trifunac, "Review: Rotations in Structural Response," *Bull. Seismol. Soc. Am.*, vol. 99, no. 2B, pp. 968–979, 2009, doi: 10.1785/0120080068.

[3] C.-C. Liu, B.-S. Huang, W. H. K. Lee, and C.-J. Lin, "Observing rotational and translational ground motions at the HGSD station in Taiwan from 2007 to 2008," *Bull. Seismol. Soc. Am.*, vol. 99, no. 2B, pp. 1228–1236, 2009.

[4] H. Igel, U. Schreiber, A. Flaws, B. Schuberth, A. Velikoseltsev, and A. Cochard, "Rotational motions induced by the M8. 1 Tokachi-oki earthquake, September 25, 2003," *Geophys. Res. Lett.*, vol. 32, no. 8, 2005.

[5] M. Takeo, "Rotational Motions Observed during an Earthquake Swarm in April 1998 Offshore Ito, Japan," *Bull. Seismol. Soc. Am.*, vol. 99, no. 2B, pp. 1457–1467, 2009, doi: 10.1785/0120080173.

[6] J. Yin, R. L. Nigbor, Q. Chen, and J. Steidl, "Engineering analysis of measured rotational ground motions at GVDA," *Soil Dyn. Earthq. Eng.*, vol. 87, pp. 125–137, 2016, doi: https://doi.org/10.1016/j.soildyn.2016.05.007.

[7] G. C. Hart, R. M. DiJulio Jr, and M. Lew, "Torsional response of high-rise buildings," *J. Struct. Div.*, vol. 101, no. 2, pp. 397–416, 1975.

[8] J. C. De la Llera and A. K. Chopra, "Accidental torsion in buildings due to base rotational excitation," *Earthq. Eng. Struct. Dyn.*, vol. 23, no. 9, pp. 1003–1021, 1994.

[9] M. D. Trifunac, M. I. Todorovska, and S. S. Ivanović, "Peak velocities and peak surface strains during Northridge, California, earthquake of 17 January 1994," *Soil Dyn. Earthq. Eng.*, vol. 15, no. 5, pp. 301–310, 1996.

[10] E. Kalkan and V. Graizer, "Coupled tilt and translational ground motion response spectra," *J. Struct. Eng.*, vol. 133, no. 5, pp. 609–619, 2007.

[11] M. R. Falamarz-Sheikhabadi, "Simplified relations for the application of rotational components to seismic design codes," *Eng. Struct.*, vol. 59, pp. 141–152, 2014.

[12] M. D. Trifunac, "The role of strong motion rotations in the response of structures near earthquake faults," *Soil Dyn. Earthq. Eng.*, vol. 29, no. 2, pp. 382–393, 2009, doi: https://doi.org/10.1016/j.soildyn.2008.04.001.

[13] R. S. Jalali, M. N. Azgomi, and M. D. Trifunac, "In-plane response of two-story structures to near-fault ground motion," *Soil Dyn. Earthq. Eng.*, vol. 55, pp. 263–274, 2013.

[14] Z. Zembaty and G. Boffi, "Effect of rotational seismic ground motion on dynamic

response of slender towers," *Eur Earthq Eng*, vol. 8, pp. 3–11, 1994.

[15]   P. A. Bońkowski, Z. Zembaty, and M. Y. Minch, "Engineering analysis of strong ground rocking and its effect on tall structures," *Soil Dyn. Earthq. Eng.*, vol. 116, pp. 358–370, 2019.

[16]   D. Basu, A. S. Whittaker, and M. C. Constantinou, "Characterizing rotational components of earthquake ground motion using a surface distribution method and response of sample structures," *Eng. Struct.*, vol. 99, pp. 685–707, 2015, doi: https://doi.org/10.1016/j.engstruct.2015.05.029.

[17]   F. Vicencio and N. A. Alexander, "A parametric study on the effect of rotational ground motions on building structural responses," *Soil Dyn. Earthq. Eng.*, vol. 118, pp. 191–206, 2019, doi: https://doi.org/10.1016/j.soildyn.2018.12.022.

[18]   F. Vicencio and N. A. Alexander, "Seismic Structure-Soil-Structure Interaction between a pair of buildings with consideration of rotational ground motions effects," *Soil Dyn. Earthq. Eng.*, vol. 163, p. 107494, 2022.

[19]   K. C. Meza Fajardo and A. S. Papageorgiou, "Response of tall buildings to base rocking induced by Rayleigh waves," *Earthq. Eng. \& Struct. Dyn.*, vol. 47, no. 8, pp. 1755–1773, 2018, doi: https://doi.org/10.1002/eqe.3040.

[20]   R. Guidotti, A. Castellani, and M. Stupazzini, "Near-Field Earthquake Strong Ground Motion Rotations and Their Relevance on Tall Buildings," *Bull. Seismol. Soc. Am.*, vol. 108, no. 3A, pp. 1171–1184, 2018, doi: 10.1785/0120170140.

[21]   S. Wu, E. Eckert, J. Huang, and D. Mccallen, "THE INFLUENCE OF ROTATIONAL COMPONENTS OF EARTHQUAKE GROUND MOTIONS ON BUILDING RESPONSE," 2021.

[22]   M. D. Trifunac, "A note on rotational components of earthquake motions on ground surface for incident body waves," *Int. J. Soil Dyn. Earthq. Eng.*, vol. 1, no. 1, pp. 11–19, 1982.

[23]   V. W. Lee and M. D. Trifunac, "Torsional accelerograms," *Int. J. Soil Dyn. Earthq. Eng.*, vol. 4, no. 3, pp. 132–139, 1985.

[24]   A. Castellani and G. Boffi, "Rotational components of the surface ground motion during an earthquake," *Earthq. Eng. Struct. Dyn.*, vol. 14, no. 5, pp. 751–767, 1986.

[25]   V. W. Lee and M. D. Trifunac, "Rocking strong earthquake accelerations," *Soil Dyn. Earthq. Eng.*, vol. 6, no. 2, pp. 75–89, 1987.

[26]   A. Castellani and G. Boffi, "On the rotational components of seismic motion," *Earthq. Eng. Struct. Dyn.*, vol. 18, no. 6, pp. 785–797, 1989.

[27]   H.-N. Li, L.-Y. Sun, and S.-Y. Wang, "Improved approach for obtaining rotational components of seismic motion," *Nucl. Eng. Des.*, vol. 232, no. 2, pp. 131–137, 2004.

[28] Z. Zembaty, "Tutorial on surface rotations from wave passage effects: stochastic spectral approach," *Bull. Seismol. Soc. Am.*, vol. 99, no. 2B, pp. 1040–1049, 2009.

[29] D. Basu, A. S. Whittaker, and M. C. Constantinou, "Estimating rotational components of ground motion using data recorded at a single station," *J. Eng. Mech.*, vol. 138, no. 9, pp. 1141–1156, 2012.

[30] M. Niazi, "Inferred displacements, velocities and rotations of a long rigid foundation located at El Centro differential array site during the 1979 Imperial Valley, California, earthquake," *Earthq. Eng. Struct. Dyn.*, vol. 14, no. 4, pp. 531–542, 1986.

[31] C. S. Oliveira and B. A. Bolt, "Rotational components of surface strong ground motion," *Earthq. Eng. \& Struct. Dyn.*, vol. 18, no. 4, pp. 517–526, 1989, doi: https://doi.org/10.1002/eqe.4290180406.

[32] B. Huang, "Ground rotational motions of the 1999 Chi-Chi, Taiwan earthquake as inferred from dense array observations," *Geophys. Res. Lett.*, vol. 30, no. 6, 2003.

[33] P. Spudich, L. K. Steck, M. Hellweg, J. B. Fletcher, and L. M. Baker, "Transient stresses at Parkfield, California, produced by the M 7.4 Landers earthquake of June 28, 1992: Observations from the UPSAR dense seismograph array," *J. Geophys. Res. Solid Earth*, vol. 100, no. B1, pp. 675–690, 1995.

[34] D. Basu, A. S. Whittaker, and M. C. Constantinou, "Extracting rotational components of earthquake ground motion using data recorded at multiple stations," *Earthq. Eng. Struct. Dyn.*, vol. 42, no. 3, pp. 451–468, 2013.

[35] M. Bouchon and K. Aki, "Strain, tilt, and rotation associated with strong ground motion in the vicinity of earthquake faults," *Bull. Seismol. Soc. Am.*, vol. 72, no. 5, pp. 1717–1738, 1982, doi: 10.1785/BSSA0720051717.

[36] G. P. Mavroeidis and A. S. Papageorgiou, "Characteristics of earthquake-induced differential ground motions in the near-fault region," 2010.

[37] Y. Cao, G. P. Mavroeidis, and M. Ashoory, "Comparison of observed and synthetic near-fault dynamic ground strains and rotations from the 2004 M w 6.0 Parkfield, California, earthquake," *Bull. Seismol. Soc. Am.*, vol. 108, no. 3A, pp. 1240–1256, 2018.

[38] Y. Cao and G. P. Mavroeidis, "A Parametric Investigation of Near-Fault Ground Strains and Rotations Using Finite-Fault Simulations," *Bull. Seismol. Soc. Am.*, vol. 109, no. 5, pp. 1758–1784, 2019, doi: 10.1785/0120190045.

[39] Y. Cao and G. P. Mavroeidis, "Simulation of near-fault ground strains and rotations from actual strike-slip earthquakes: case studies of the 2004 M w 6.0 Parkfield, the 1979 M w 6.5 Imperial Valley and the 1999 M w 7.5 Izmit earthquakes," *Geophys. J. Int.*, vol. 226, no. 3, pp. 1920–1947, 2021.

[40] H. Johansen, A. Rodgers, N. A. Petersson, D. McCallen, B. Sjogreen, and M.

Miah, "Toward exascale earthquake ground motion simulations for near-fault engineering analysis," *Comput. Sci. Eng.*, vol. 19, no. 5, pp. 27–37, 2017.

[41] D. McCallen *et al.*, "EQSIM—A multidisciplinary framework for fault-to-structure earthquake simulations on exascale computers part I: Computational models and workflow," *Earthq. Spectra*, vol. 37, no. 2, pp. 707–735, 2021.

[42] D. McCallen, F. Petrone, M. Miah, A. Pitarka, A. Rodgers, and N. Abrahamson, "EQSIM—A multidisciplinary framework for fault-to-structure earthquake simulations on exascale computers, part II: Regional simulations of building response," *Earthq. Spectra*, vol. 37, no. 2, pp. 736–761, 2021.

[43] H. Igel, M. Käser, and M. Stupazzini, "Seismic Wave Propagation in Media with Complex Geometries, Simulation of." 2009.

[44] M. Stupazzini, R. Paolucci, and H. Igel, "Near-fault earthquake ground-motion simulation in the Grenoble valley by a high-performance spectral element code," *Bull. Seismol. Soc. Am.*, vol. 99, no. 1, pp. 286–301, 2009.

[45] I. Mazzieri, M. Stupazzini, R. Guidotti, and C. Smerzini, "SPEED: SPectral Elements in Elastodynamics with Discontinuous Galerkin: A non-conforming approach for 3D multi-scale problems," *Int. J. Numer. Methods Eng.*, vol. 95, no. 12, pp. 991–1010, 2013.

[46] N. A. Petersson and B. Sjögreen, "Stable and efficient modeling of anelastic attenuation in seismic wave propagation," *Commun. Comput. Phys.*, vol. 12, no. 1, pp. 193–225, 2012.

[47] J. Bielak, K. Loukakis, Y. Hisada, and C. Yoshimura, "Domain reduction method for three-dimensional earthquake modeling in localized regions, Part I: Theory," *Bull. Seismol. Soc. Am.*, vol. 93, no. 2, pp. 817–824, 2003.

[48] F. McKenna, M. H. Scott, and G. L. Fenves, "Nonlinear finite-element analysis software architecture using object composition," *J. Comput. Civ. Eng.*, vol. 24, no. 1, pp. 95–107, 2010.

[49] R. Graves and A. Pitarka, "Refinements to the Graves and Pitarka (2010) broadband ground-motion simulation method," *Seismol. Res. Lett.*, vol. 86, no. LLNL-JRNL-741227, 2014.

[50] P. Spudich and J. B. Fletcher, "Observation and Prediction of Dynamic Ground Strains, Tilts, and Torsions Caused by the Mw 6.0 2004 Parkfield, California, Earthquake and Aftershocks, Derived from UPSAR Array Observations," *Bull. Seismol. Soc. Am.*, vol. 98, no. 4, pp. 1898–1914, 2008, doi: 10.1785/0120070157.

[51] M. Stupazzini, J. de la Puente, C. Smerzini, M. Käser, H. Igel, and A. Castellani, "Study of Rotational Ground Motion in the Near-Field Region," *Bull. Seismol. Soc. Am.*, vol. 99, no. 2B, pp. 1271–1286, 2009, doi: 10.1785/0120080153.

[52] H. Wang, H. Igel, F. Gallovič, and A. Cochard, "Source and Basin Effects on

Rotational Ground Motions: Comparison with Translations," *Bull. Seismol. Soc. Am. - BULL Seism. SOC AMER*, vol. 99, May 2009, doi: 10.1785/0120080115.

[53] V. Graizer, "Deformations and Rotational Motions Extracted from Delaney Park Downhole Array Recordings," in *AGU Fall Meeting Abstracts*, Dec. 2019, vol. 2019, pp. S21G-0588.

[54] M. A. Santoyo, "Finite fault analysis and near-field dynamic strain and rotation estimates due to the 11/05/2011 (Mw5. 2) Lorca earthquake, south-eastern Spain," *Bull. Earthq. Eng.*, vol. 12, no. 5, pp. 1855–1870, 2014.

[55] S. Wu, E. Eckert, J. Huang, and D. Mccallen, "Evaluation of the domain reduction method applied to broad-band, near-fault earthquake ground motions with inter-code comparisons," *Tech. Rep.*, 2020.

[56] P. A. Bońkowski, Z. Zembaty, and M. Y. Minch, "Time history response analysis of a slender tower under translational-rocking seismic excitations," *Eng. Struct.*, vol. 155, pp. 387–393, 2018, doi: https://doi.org/10.1016/j.engstruct.2017.11.042.

[57] V. K. Gupta and M. D. Trifunac, "Response of multistoried buildings to ground translation and rocking during earthquakes," *Probabilistic Eng. Mech.*, vol. 5, no. 3, pp. 138–145, 1990, doi: https://doi.org/10.1016/0266-8920(90)90005-5.

[58] E. M. Rathje, F. Faraj, S. Russell, and J. D. Bray, "Empirical relationships for frequency content parameters of earthquake ground motions," *Earthq. Spectra*, vol. 20, no. 1, pp. 119–144, 2004.

[59] M. Kumar, J. M. Castro, P. J. Stafford, and A. Y. Elghazouli, "Influence of the mean period of ground motion on the inelastic dynamic response of single and multi degree of freedom systems," *Earthq. Eng. Struct. Dyn.*, vol. 40, no. 3, pp. 237–256, 2011.

[60] M. Kumar, P. J. Stafford, and A. Y. Elghazouli, "Influence of ground motion characteristics on drift demands in steel moment frames designed to Eurocode 8," *Eng. Struct.*, vol. 52, pp. 502–517, 2013.

[61] R. Song, Y. Li, and J. W. van de Lindt, "Impact of earthquake ground motion characteristics on collapse risk of post-mainshock buildings considering aftershocks," *Eng. Struct.*, vol. 81, pp. 349–361, 2014.

[62] E. M. Rathje, N. A. Abrahamson, and J. D. Bray, "Simplified frequency content estimates of earthquake ground motions," *J. Geotech. geoenvironmental Eng.*, vol. 124, no. 2, pp. 150–159, 1998.